

Unravelling the anomalous gauge boson couplings in ZW^\pm production at the LHC and the role of spin-1 polarizations

Rafiqul Rahaman and Ritesh K. Singh

Department of Physical Sciences, Indian Institute of Science Education and Research Kolkata, Mohanpur, 741246, India

E-mail: rr13rs033@iiserkol.ac.in, ritesh.singh@iiserkol.ac.in

ABSTRACT: We study the anomalous triple gauge boson couplings (aTGC) in ZW^\pm production in $3l + \cancel{E}_T$ channel at the LHC for $\sqrt{s} = 13$ TeV. We use cross sections, azimuthal asymmetry, forward-backward asymmetry, and polarization asymmetries of Z and reconstructed W to estimate simultaneous limits on the anomalous couplings for both the effective vertex formalism as well as the effective operator approach using the Markov-chain–Monte-Carlo (MCMC) method for luminosities 35.9 fb^{-1} , 100 fb^{-1} , 300 fb^{-1} , 1000 fb^{-1} , and 3000 fb^{-1} . The trilepton invariant mass (m_{3l}) and the transverse momentum of Z ($p_T(Z)$) are found to be sensitive to the aTGC for the cross sections as well as for the asymmetries. We observed that the asymmetries significantly improve the measurement of anomalous couplings at the high-luminosity large hadron collider (LHC) if a deviation from the Standard Model (SM) is observed.

KEYWORDS: Polarization of Z and W boson, anomalous triple gauge boson couplings (aTGC), neutrino reconstruction, MCMC

Contents

1	Introduction	1
2	Signal cross sections and their sensitivity to anomalous couplings	4
3	Polarization observables of Z and W^\pm along with other angular asymmetries	8
4	Measurement of the anomalous couplings	14
4.1	Limits on the couplings	14
4.2	The role of asymmetries in parameter extraction	19
5	Conclusion	20
A	Fitting procedure in obtaining observables as a function of couplings	21
B	Standard Model values of the asymmetries and polarizations	24

1 Introduction

After the discovery of Higgs [1, 2], the Large Hadron Collider (LHC) has been looking for new physics beyond the SM (BSM) needed to address many open questions such as neutrino oscillation, dark matter, baryogenesis, etc. with higher energies and higher luminosities. Unfortunately, no new physics has been found [3–7] except a few fluctuations (e.g., Refs. [8–10]). One could expect that the new physics scale is too heavy to be directly explored by the LHC, and they may leave some footprints in the available energy range. They will modify the structure of the SM vertices or bring some new vertices, often through higher-dimensional operators with the SM fields. These new vertices and/or the extra contribution to the SM vertices are termed as anomalous in the sense that they are not present in the SM at leading order (LO). The electroweak sector will get affected by the anomalous bosonic self-couplings, which alter the paradigm of electroweak symmetry breaking (EWSB). To understand the EWSB mechanism, one needs precise measurements of the couplings in the bosonic sector of the SM. Here, we choose to focus on the charge sector by probing the WWZ anomalous couplings in the ZW^\pm production at the LHC. The WWZ anomalous triple gauge boson couplings (aTGC) may be obtained by higher dimension effective operators made out of SM fields suppressed by a new physics scale Λ . The effective Lagrangian including the higher dimension effective operators (\mathcal{O}) to the SM Lagrangian (\mathcal{L}_{SM}) is treated to be

$$\mathcal{L}_{eft} = \mathcal{L}_{SM} + \sum_i \frac{c_i^{(6)}}{\Lambda^2} \mathcal{O}_i^{(6)} + \sum_i \frac{c_i^{(8)}}{\Lambda^4} \mathcal{O}_i^{(8)} + \dots, \quad (1.1)$$

with $c_i^{\mathcal{O}(6,8)}$ being the couplings of the dimension-(6,8) operators $\mathcal{O}_i^{(6,8)}$. The effective operators in the Hagiwara-Ishihara- Szalapski-Zeppenfeld (HISZ) basis up to dimension-6 contributing to WWZ/γ couplings, in general, are [11, 12]

$$\begin{aligned}\mathcal{O}_{WWW} &= \text{Tr}[W_{\mu\nu}W^{\nu\rho}W_\rho^\mu] , \\ \mathcal{O}_W &= (D_\mu\Phi)^\dagger W^{\mu\nu}(D_\nu\Phi) , \\ \mathcal{O}_B &= (D_\mu\Phi)^\dagger B^{\mu\nu}(D_\nu\Phi) , \\ \mathcal{O}_{\widetilde{WWW}} &= \text{Tr}[\widetilde{W}_{\mu\nu}W^{\nu\rho}W_\rho^\mu] , \\ \mathcal{O}_{\widetilde{W}} &= (D_\mu\Phi)^\dagger \widetilde{W}^{\mu\nu}(D_\nu\Phi) .\end{aligned}\tag{1.2}$$

Among these operators \mathcal{O}_{WWW} , \mathcal{O}_W and \mathcal{O}_B are CP -even, while $\mathcal{O}_{\widetilde{WWW}}$ and $\mathcal{O}_{\widetilde{W}}$ are CP -odd. On the other hand, the WWZ anomalous couplings may be parametrized in a model independent way with the most general Lorentz invariant form factors or vertex factors given by [13]

$$\begin{aligned}\mathcal{L}_{WWZ} &= ig_{WWZ} \left[(1 + \Delta g_1^Z) (W_\mu^+ W^{-\mu} - W^{+\mu} W_{\mu\nu}^-) Z^\nu + \frac{\lambda^Z}{m_W^2} W_\mu^{+\nu} W_\nu^{-\rho} Z_\rho^\mu \right. \\ &\quad \left. + \frac{\widetilde{\lambda}^Z}{m_W^2} W_\mu^{+\nu} W_\nu^{-\rho} \widetilde{Z}_\rho^\mu + (1 + \Delta \kappa^Z) W_\mu^+ W_\nu^- Z^{\mu\nu} + \widetilde{\kappa}^Z W_\mu^+ W_\nu^- \widetilde{Z}^{\mu\nu} \right] ,\end{aligned}\tag{1.3}$$

where $W_{\mu\nu}^\pm = \partial_\mu W_\nu^\pm - \partial_\nu W_\mu^\pm$, $Z_{\mu\nu} = \partial_\mu Z_\nu - \partial_\nu Z_\mu$, $\widetilde{Z}^{\mu\nu} = 1/2\epsilon^{\mu\nu\rho\sigma}Z_{\rho\sigma}$, and the overall coupling constants is given as $g_{WWZ} = -g \cos \theta_W$, θ_W being the weak mixing angle. The couplings Δg_1^Z , $\Delta \kappa^Z$ and λ^Z of Eq. (1.3) are CP -even, while $\widetilde{\kappa}^Z$ and $\widetilde{\lambda}^Z$ are CP -odd in nature. All the anomalous couplings vanish in the SM. In the $SU(2) \times U(1)$ gauge group, the coupling ($c_i^{\mathcal{L}}$) of the Lagrangian in Eq. (1.3) are related to the couplings $c_i^{\mathcal{O}}$ of the operators in Eq. (1.2) as [11, 12, 14]

$$\begin{aligned}\Delta g_1^Z &= c_W \frac{m_Z^2}{2\Lambda^2} , \\ \lambda^Z &= c_{WWW} \frac{3g^2 m_W^2}{2\Lambda^2} , \\ \widetilde{\lambda}^Z &= c_{\widetilde{WWW}} \frac{3g^2 m_W^2}{2\Lambda^2} , \\ \Delta \kappa^Z &= (c_W - c_B \tan^2 \theta_W) \frac{m_W^2}{2\Lambda^2} , \\ \widetilde{\kappa}^Z &= -c_{\widetilde{W}} \tan^2 \theta_W \frac{m_W^2}{2\Lambda^2} .\end{aligned}\tag{1.4}$$

We label the anomalous couplings of three scenarios for later uses as follows: The couplings of the operators in Eq. (1.2), the couplings of effective vertices in \mathcal{L}_{WWV} in Eq. (1.3) and the vertex couplings translated from the operators in Eq. (1.4) are labelled as $c_i^{\mathcal{O}}$, $c_i^{\mathcal{L}}$, and $c_i^{\mathcal{L}^g}$, respectively.

These anomalous gauge boson self-couplings may be obtained from some high scale new physics such as MSSM [15–17], extra dimension [18, 19], Georgi-Machacek model [20], etc. by integrating out the heavy degrees of freedom. Some of these couplings can also be obtained at loop level within the SM [21, 22]. There have been a lot of studies to probe the anomalous WWZ/γ couplings in the effective operator method as well as in the effective vertex factor approach subjected to $SU(2) \times U(1)$ invariance for various colliders: for e^+e^- linear collider [13, 23–34], for

the Large Hadron electron collider (LHeC) [35–37], $e\text{-}\gamma$ collider [38] and for the LHC [30, 31, 39–52]. Some CP -odd WWV couplings have been studied in Refs. [33, 48]. Direct measurement of these charged aTGC has been performed at the LEP [53–56], Tevatron [57, 58], LHC [59–74] and Tevatron-LHC [75]. The most stringent constraints on the operators ($c_i^{\mathcal{O}}$) are obtained in Ref. [72] for CP -even ones and in Ref. [61] for CP -odd ones, and they are listed in Table 1. These limits translated to the effective vertices ($c_i^{\mathcal{L}_g}$) are also given in Table 1.

Table 1: The list of tightest constraints observed on the effective operators and the effective vertices in $SU(2) \times U(1)$ gauge at 95% C.L. from experiments.

$c_i^{\mathcal{O}}$	Limits (TeV^{-2})	Remark
$\frac{c_{WWW}}{\Lambda^2}$	$[-1.58, +1.59]$	CMS $\sqrt{s} = 13$ TeV, $\mathcal{L} = 35.9 \text{ fb}^{-1}$, $SU(2) \times U(1)$ [72]
$\frac{c_W}{\Lambda^2}$	$[-2.00, +2.65]$	CMS [72]
$\frac{c_B}{\Lambda^2}$	$[-8.78, +8.54]$	CMS [72]
$\frac{c_{\widetilde{WWW}}}{\Lambda^2}$	$[-11, +11]$	ATLAS $\sqrt{s} = 7(8)$ TeV, $\mathcal{L} = 4.7(20.2) \text{ fb}^{-1}$ [61]
$\frac{c_{\widetilde{W}}}{\Lambda^2}$	$[-580, 580]$	ATLAS [61]
$c_i^{\mathcal{L}_g}$	Limits ($\times 10^{-2}$)	Remark
λ^Z	$[-0.65, +0.66]$	CMS [72]
Δg_1^Z	$[-0.61, +0.74]$	CMS [72]
$\Delta \kappa^Z$	$[-0.79, +0.82]$	CMS [72]
$\widetilde{\lambda}^Z$	$[-4.7, +4.6]$	ATLAS [61]
$\widetilde{\kappa}^Z$	$[-14, -1]$	DELPHI (LEP2) $\sqrt{s} = 189\text{-}209$ GeV, $\mathcal{L} = 520 \text{ pb}^{-1}$ [55]

In this article, we intend to study the WWZ anomalous couplings in ZW^\pm production at the LHC at $\sqrt{s} = 13$ TeV using the cross sections, forward-backward asymmetries, and polarizations asymmetries [53, 76–81] of Z and W^\pm in the $3l + \cancel{E}_T$ channel. The polarizations of Z and W have been used recently for various BSM studies [82–88] along with studies of anomalous gauge boson couplings [53, 80, 89, 90]. The polarizations of W^\pm/Z have been estimated earlier in ZW^\pm production [91–93] and also have been measured recently at the LHC [94] in the SM. We note that the ZW^\pm processes also contain anomalous couplings other than aTGC, such as the anomalous $Zq\bar{q}$ couplings, and they affect the measurement of aTGC [28, 46, 52]. However, the main aim of this paper is to demonstrate the usefulness of polarization observables in probing possible new physics. For simplicity, we restrict our analysis to possible anomalous couplings only in the bosonic sector of the SM.

We will begin in Sect. 2 by providing the estimates of the cross sections for CMS fiducial phase-space by MATRIX [95], MADGRAPH5_aMC@NLO [96] and investigate their sensitivities to the anomalous couplings. Section 3 is devoted to polarization asymmetries of Z and W and the

reconstruction of longitudinal momenta of the missing neutrino. In Sect. 4, we perform a simultaneous analysis using the Markov-chain–Monte-Carlo (MCMC) to obtain limits on the anomalous couplings along with a toy measurement of *non-zero* aTGC and conclude in Sect. 5.

2 Signal cross sections and their sensitivity to anomalous couplings

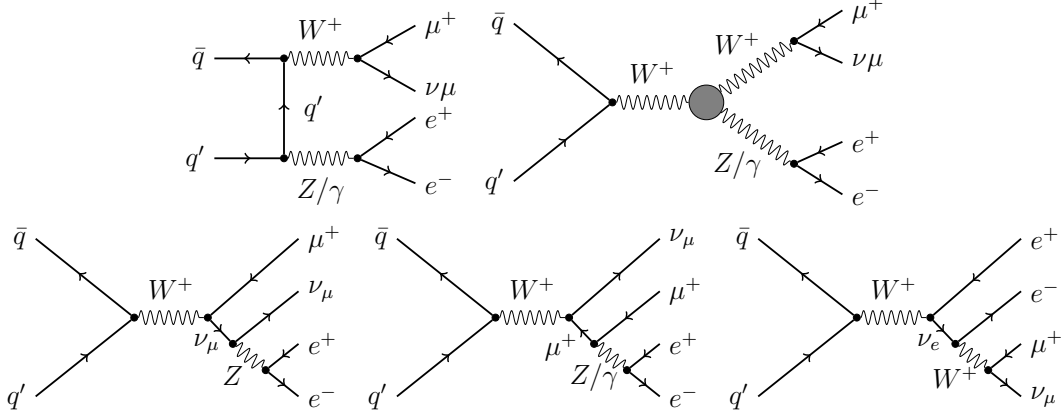


Figure 1: Sample of Born level Feynman diagrams for ZW^+ production in the $e^+e^-\mu^+\nu_\mu$ channel at the LHC. The diagrams for ZW^- can be obtained by charge conjugation. The shaded blob represents the presence of anomalous WWV couplings on top of SM.

Table 2: The theoretical estimates and experimental measurements of the cross sections of ZW^\pm production in the $e^+e^-\mu^\pm\nu_\mu/\bar{\nu}_\mu$ channels at $\sqrt{s} = 13$ TeV at the LHC for CMS fiducial phase-space. The uncertainties in the theoretical estimates are due to scale variation.

Process	Obtained at	σ_{LO} (fb)	σ_{NLO} (fb)	σ_{NNLO} (fb)
$pp \rightarrow e^+e^-\mu^+\nu_\mu$	MATRIX	$22.08^{+5.2\%}_{-6.2\%}$	$43.95^{+5.4\%}_{-4.3\%}$	$48.55^{+2.2\%}_{-2.0\%}$
	mg5_aMC	$22.02^{+6.1\%}_{-7.2\%}$	$43.63^{+6.6\%}_{-6.6\%}$	—
$pp \rightarrow e^+e^-\mu^-\bar{\nu}_\mu$	MATRIX	$14.45^{+5.6\%}_{-6.7\%}$	$30.04^{+5.6\%}_{-4.5\%}$	$33.39^{+2.3\%}_{-2.1\%}$
	mg5_aMC	$14.38^{+6.4\%}_{-7.6\%}$	$29.85^{+6.8\%}_{-6.8\%}$	—
$pp \rightarrow 3l + \cancel{E}_T$	MATRIX [97]	$148.4^{+5.4\%}_{-6.4\%}$	$301.4^{+5.1\%}_{-4.4\%}$	$334.3^{+2.3\%}_{-2.1\%}$
$pp \rightarrow 3l + \cancel{E}_T$	CMS [98]	$258.0 \pm 8.1\%$ (stat) $^{+7.4\%}_{-7.7\%}$ (syst) ± 3.1 (lumi)		

The processes of interest are the ZW^\pm production in the $3l + \cancel{E}_T$ channel at the LHC. The representative Feynman diagrams at Born level are displayed in Fig. 1 containing doubly-resonant processes (*upper-row*) as well as singly-resonant processes (*lower-row*). The presence of anomalous WWZ couplings is shown by the shaded blob. While this may contain the $WW\gamma$ couplings due

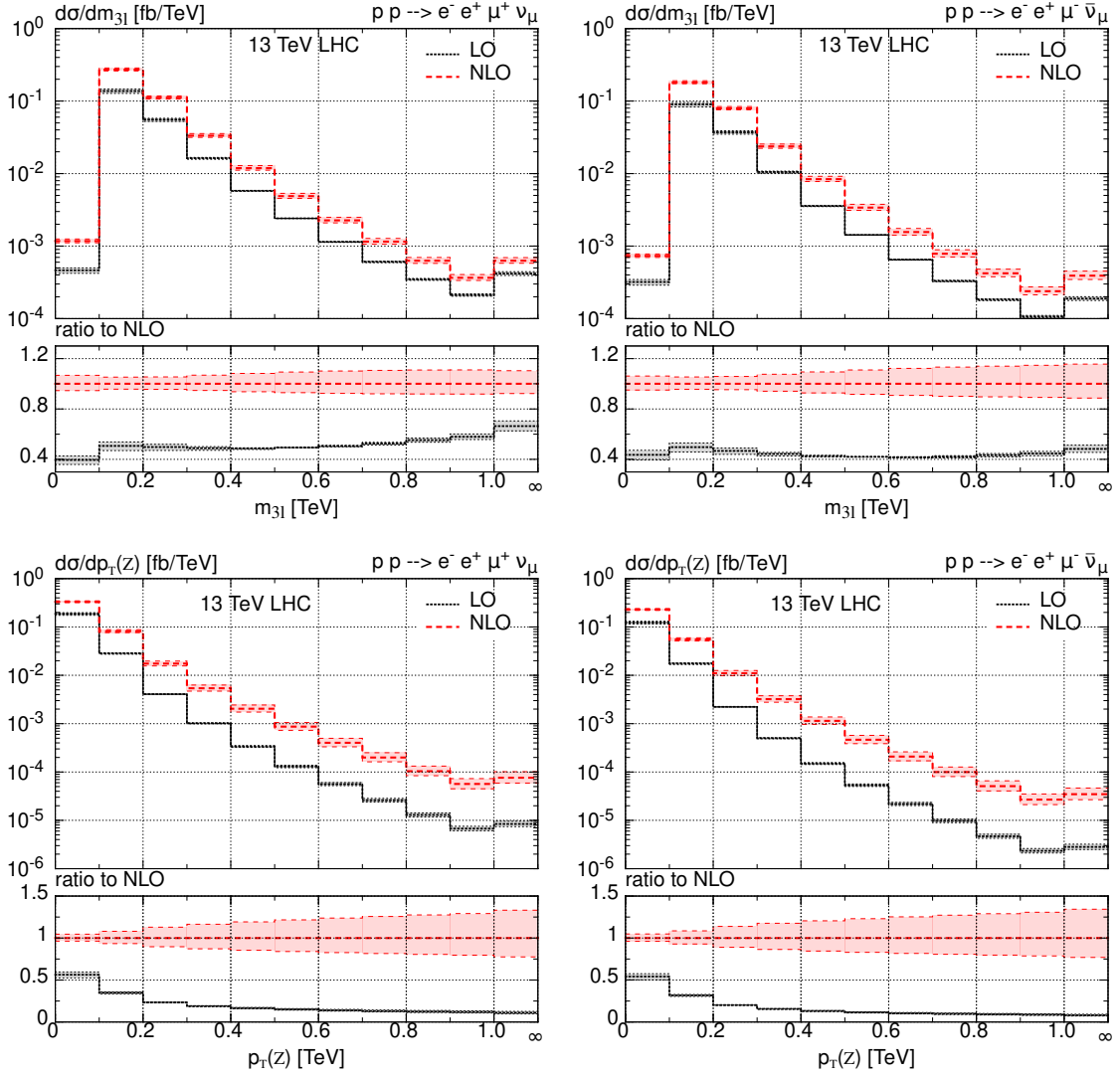


Figure 2: The differential distributions of m_{3l} (top-row) and $p_T(Z)$ (bottom-row) in the ZW^+ (left-column) and ZW^- (right-column) production in the $e^+e^-\mu^\pm + \cancel{E}_T$ channel at the LHC for $\sqrt{s} = 13$ TeV at LO and NLO in QCD obtained using MATRIX [95, 97, 99–104] for CMS fiducial phase-space.

to the off-shell γ , this has been cut out by Z selection cuts, described later. The leading order result ($\sigma_{\text{LO}}^{\text{th}} = 148.4$ fb estimated by MATRIX in Ref. [97]) for the $3l + \cancel{E}_T$ cross section at the LHC is way below the measured cross section at the LHC ($\sigma_{\text{exp}}^{\text{CMS}} = 258$ fb measured by CMS [98]). Higher-order corrections to the tree level result are thus necessary. The next-to-leading order (NLO) corrections in QCD appear in the vertices connected to the quarks (see, Fig. 1) with either QCD loops or QCD radiations from the quarks. The SM cross sections of ZW^\pm production in the $e^+e^-\mu^\pm$ channel obtained by MATRIX and MADGRAPH5_aMC@NLO v2.6.4 (mg5_aMC) for $\sqrt{s} = 13$ TeV for the CMS fiducial phase-phase region are presented in Table 2. The CMS fiducial phase-phase

region [98] is given by

$$p_T(l_{Z,1}) > 20 \text{ GeV}, \quad p_T(l_{Z,2}) > 10 \text{ GeV}, \quad p_T(l_W) > 20 \text{ GeV}, \\ |\eta_l| < 2.5, \quad 60 \text{ GeV} < m_{l^+l^-} < 120 \text{ GeV}, \quad m_{l^+l^-} > 4 \text{ GeV}. \quad (2.1)$$

We use the values of the SM input parameters the same as used in Ref. [97] (default in MATRIX). A fixed renormalization (μ_R) and factorization (μ_F) scale of $\mu_R = \mu_F = \mu_0 = \frac{1}{2}(m_Z + m_W)$ is used, and the uncertainties are estimated by varying the μ_R and μ_F in the range of $0.5\mu_0 \leq \mu_R, \mu_F \leq 2\mu_0$, with the constraint $0.5 \leq \mu_R/\mu_F \leq 2$ and shown in Table 2. We use the NNPDF3.0 [105] sets of parton distribution functions (PDFs) with $\alpha_s(m_Z) = 0.118$ for our calculations. The combined result for all leptonic channels given in Ref. [97] and the measured cross section by CMS [98] are also presented in the same table. The uncertainties in the theoretical estimates are due to scale variation. The result obtained by MATRIX and mg5_aMC matches quite well at both LO and NLO level. The NLO corrections have increased the LO cross section by up to 100 % and the next-to-next-to-leading order (NNLO) cross section is further increased by 10 % from the NLO value. The higher order corrections to the cross section vary with kinematical variable like m_{3l} and $p_T(Z)$, as shown in Fig. 2 obtained by MATRIX [95, 97, 99–104]. The lower panels display the respective bin-by-bin ratios to the NLO central predictions. The NLO to LO ratio does not appear to be constant over the range of m_{3l} and $p_T(Z)$. Thus a simple k -factor with LO events can not be used as a proxy for NLO events. We use results from mg5_aMC, including NLO QCD corrections, for our analysis in the rest of the paper.

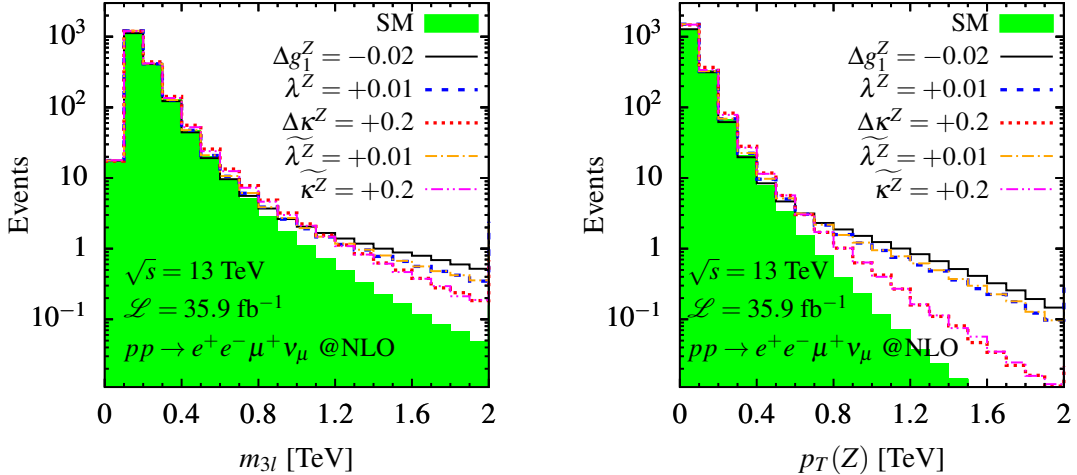


Figure 3: The differential distributions of m_{3l} and $p_T(Z)$ in the W^+Z production in the $e^+e^-\mu^+\nu_\mu$ channel at the LHC at $\sqrt{s} = 13 \text{ TeV}$ and $\mathcal{L} = 35.9 \text{ fb}^{-1}$ at NLO in QCD for SM and five benchmark anomalous couplings.

The signals for the $e^+e^-\mu^+$ and $e^+e^-\mu^-$ are generated separately using mg5_aMC at NLO in QCD for SM as well as SM including aTGC. We use the FeynRules [106] to generate QCD NLO UFO model of the Lagrangian in Eq. (1.3) for mg5_aMC. These signals are then used as a proxy for the $3l + \cancel{E}_T$ final state up to a factor of four for the four channels. For these, the p_T cut for e^\pm and

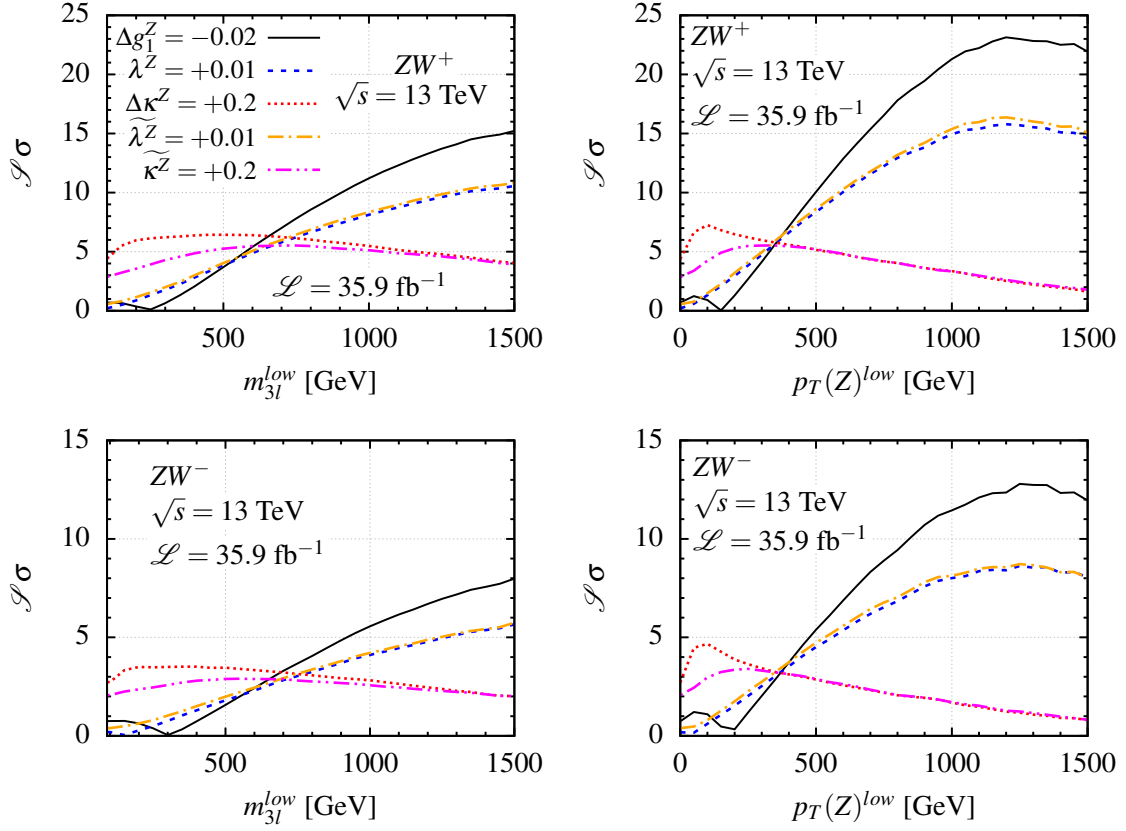


Figure 4: The sensitivities of cross sections to the five benchmark aTGC as a function of the lower cut on m_{3l} and $p_T(Z)$ in the ZW^\pm production at the LHC at $\sqrt{s} = 13$ TeV and $\mathcal{L} = 35.9$ fb $^{-1}$.

μ^\pm are kept at the same value, i.e., $p_T(l) > 10$ GeV. We use a threshold for the tripleton invariant mass (m_{3l}) of 100 GeV to select the doubly resonant contribution of tripleton final state. Later we will see that a cut of $m_{3l} \geq 100$ GeV is required to improve the sensitivities of the observables to the anomalous couplings. The event selection cuts for this analysis are thus,

$$p_T(l) > 10 \text{ GeV}, \quad |\eta_l| < 2.5, \quad 60 \text{ GeV} < m_{l^+l^-} < 120 \text{ GeV}, \quad m_{l^+l^-} > 4 \text{ GeV}, \quad m_{3l} > 100 \text{ GeV} . \quad (2.2)$$

We explore the effect of aTGC in the distributions of m_{3l} and $p_T(Z)$ in both ZW^+ and ZW^- production and show them in Fig. 3. The distribution of m_{3l} in the *left-panel* and $p_T(Z)$ in the *right-panel* in the $e^+e^-\mu^+\nu_\mu$ channel are shown for SM (*filled/green*) and five anomalous benchmark couplings¹ of $\Delta g_1^Z = -0.02$ (*solid/black*), $\lambda^Z = +0.01$ (*dashed/blue*), $\Delta \kappa^Z = +0.2$ (*dotted/red*), $\tilde{\lambda}^Z = +0.01$ (*dash-dotted/orange*) and $\tilde{\kappa}^Z = +0.2$ (*dashed-dotdotted/magenta*) with events normalized to an integrated luminosity of $\mathcal{L} = 35.9$ fb $^{-1}$. The higher m_{3l} and higher $p_T(Z)$ seem to have higher sensitivity to the anomalous couplings which is due to higher momentum transfer at higher energies, for example see Ref. [34]. We study the sensitivity of total cross section

¹For each of these benchmark couplings, only one of the couplings is set to non-zero value such that it leads to $\sim 1\sigma$ deviation in the total cross section. More benchmark scenarios (~ 100) with more than one parameters set to non-zero values at a time are also considered in later sections.

to the anomalous couplings by varying lower cut on m_{3l} and $p_T(Z)$ for the above mentioned five benchmark scenarios. The sensitivity of an observable $\mathcal{O}(c_i)$ to coupling c_i is defined as

$$\mathcal{S}\mathcal{O}(c_i) = \frac{|\mathcal{O}(c_i) - \mathcal{O}(c_i = 0)|}{\delta\mathcal{O}}, \quad (2.3)$$

where $\delta\mathcal{O}$ is the estimated error in \mathcal{O} . For cross sections and asymmetries, the errors are

$$\delta\sigma = \sqrt{\frac{\sigma}{\mathcal{L}} + (\varepsilon_\sigma\sigma)^2} \quad \text{and} \quad \delta A_i = \sqrt{\frac{1 - A_i^2}{\mathcal{L} \times \sigma} + \varepsilon_A^2}, \quad (2.4)$$

where \mathcal{L} is the integrated luminosity and ε_σ and ε_A are the systematic uncertainties for the cross section and the asymmetries, respectively. The sensitivities of the cross sections, ignoring the systematic uncertainty, for the five benchmark cases (as used in Fig. 3) are shown in Fig. 4 for ZW^+ in the *upper-row* and for ZW^- in the *lower-row* as a function of lower cut of m_{3l} (*left-column*) and $p_T(Z)$ (*right-column*) for luminosity of $\mathcal{L} = 35.9 \text{ fb}^{-1}$. It is clear that the sensitivities increase as the cut increases for both m_{3l} and $p_T(Z)$ for couplings Δg_1^Z , λ^Z and $\widetilde{\lambda}^Z$, while they decrease just after $\sim 150 \text{ GeV}$ of cuts for the couplings $\Delta\kappa^Z$ and $\widetilde{\kappa}^Z$. This can also be seen in Fig. 3 where $\Delta\kappa^Z$ and $\widetilde{\kappa}^Z$ contribute more than other three couplings for $m_{3l} < 0.8 \text{ TeV}$ and $p_T(Z) < 0.6 \text{ TeV}$. Taking hints from Fig. 4, we identify four bins in m_{3l} - $p_T(Z)$ plane to maximize the sensitivity of all the couplings. These four bins are given by,

$$\begin{aligned} \text{Bin}_{11} &: 400 \text{ GeV} < m_{3l} < 1500 \text{ GeV}, 200 \text{ GeV} < p_T(Z) < 1200 \text{ GeV} , \\ \text{Bin}_{12} &: 400 \text{ GeV} < m_{3l} < 1500 \text{ GeV}, p_T(Z) > 1200 \text{ GeV} , \\ \text{Bin}_{21} &: m_{3l} > 1500 \text{ GeV}, 200 \text{ GeV} < p_T(Z) < 1200 \text{ GeV} , \\ \text{Bin}_{22} &: m_{3l} > 1500 \text{ GeV}, p_T(Z) > 1200 \text{ GeV} . \end{aligned} \quad (2.5)$$

The sensitivities of the cross sections to the benchmark anomalous couplings are calculated in the said four bins for luminosity of $\mathcal{L} = 35.9 \text{ fb}^{-1}$ and they are shown in Table 3 in both ZW^+ and ZW^- productions. As expected, we see that Bin_{22} has the higher sensitivity to couplings Δg_1^Z , λ^Z and $\widetilde{\lambda}^Z$, while Bin_{11} has higher, but comparable sensitivity to couplings $\Delta\kappa^Z$ and $\widetilde{\kappa}^Z$. The simultaneous cuts on both the variable have increased the sensitivity by a significant amount as compared to the individual cuts. For example, Fig. 4 shows that cross section in ZW^+ has a maximum sensitivity of 15 and 22 on $\Delta g_1^Z = -0.02$ for individual m_{3l} and $p_T(Z)$ lower cuts, respectively. While imposing simultaneous lower cuts on both the variable, the same sensitivity increases to 44.5 (in Bin_{22}).

At the LHC, the other contributions to the $3l + \cancel{E}_T$ channel come from the production of ZZ , $Z\gamma$, $Z + j$, $t\bar{t}$, Wt , $WW + j$, $t\bar{t} + V$, tZ , VVV as has been studied by CMS [74, 98] and ATLAS [94, 107]. The total non- ZW contributions listed above is about 40 % of the ZW contributions [98]. We include these extra contributions to the cross sections while estimating limits on the anomalous couplings in Sect. 4.

3 Polarization observables of Z and W^\pm along with other angular asymmetries

Being a spin-1 particle, the Z/W (V) offers eight additional observables related to their eight degrees of polarizations apart from their production cross sections. The angular distributions of the

Table 3: The sensitivities of the cross sections on the five benchmark aTGC in the four bins (see Eq. (2.5)) of m_{3l} and $p_T(Z)$ in the ZW^\pm productions at the LHC at $\sqrt{s} = 13$ TeV and $\mathcal{L} = 35.9$ fb $^{-1}$.

	ZW^+				ZW^-			
aTGC	Bin_{11}	Bin_{12}	Bin_{21}	Bin_{22}	Bin_{11}	Bin_{12}	Bin_{21}	Bin_{22}
$\Delta g_1^Z = -0.02$	1.17	1.14	7.52	44.5	0.32	2.10	3.95	23.19
$\lambda^Z = 0.01$	3.08	5.37	6.08	26.2	1.58	2.63	3.32	13.68
$\Delta \kappa^Z = 0.2$	8.52	0.50	3.28	4.87	5.01	0.15	1.64	2.40
$\widetilde{\lambda}^Z = 0.01$	3.20	5.56	6.18	27.2	1.70	2.69	3.37	13.83
$\widetilde{\kappa}^Z = 0.2$	6.50	0.60	3.15	4.89	3.86	0.22	1.65	2.36

daughter particle reveal the polarizations of the mother particle V . The normalized decay angular distribution of the daughter fermion f (l_Z/l_W) from the decay of V is given by [78]

$$\begin{aligned}
\frac{1}{\sigma} \frac{d\sigma}{d\Omega_f} = & \frac{3}{8\pi} \left[\left(\frac{2}{3} - (1-3\delta) \frac{T_{zz}}{\sqrt{6}} \right) + \alpha p_z \cos \theta_f + \sqrt{\frac{3}{2}} (1-3\delta) T_{zz} \cos^2 \theta_f \right. \\
& + \left(\alpha p_x + 2\sqrt{\frac{2}{3}} (1-3\delta) T_{xz} \cos \theta_f \right) \sin \theta_f \cos \phi_f \\
& + \left(\alpha p_y + 2\sqrt{\frac{2}{3}} (1-3\delta) T_{yz} \cos \theta_f \right) \sin \theta_f \sin \phi_f \\
& + (1-3\delta) \left(\frac{T_{xx} - T_{yy}}{\sqrt{6}} \right) \sin^2 \theta_f \cos(2\phi_f) \\
& \left. + \sqrt{\frac{2}{3}} (1-3\delta) T_{xy} \sin^2 \theta_f \sin(2\phi_f) \right]. \tag{3.1}
\end{aligned}$$

Here θ_f , ϕ_f are the polar and the azimuthal orientation of the fermion f , in the rest frame of the particle (V) with its would be momentum along the z -direction. For massless final state fermions, we have $\delta = 0$ and $\alpha = (R_f^2 - L_f^2)/(R_f^2 + L_f^2)$ for Z with $Zf\bar{f}$ coupling to be $\gamma^\mu (L_f P_L + R_f P_R)$ and $\alpha = -1$ for W^\pm . The quantities p_x , p_y , and p_z are the three vector polarizations and T_{xy} , T_{xz} , T_{yz} , $T_{xx} - T_{yy}$, and T_{zz} are the five independent tensor polarizations of the particle V . These polarizations p_i and T_{ij} are calculable from asymmetries constructed from the decay angular information of lepton using Eq. (3.1). For example, the polarization parameters p_z and T_{xz} can be calculated from the asymmetries A_z and A_{xz} , respectively, as

$$\begin{aligned}
A_z = & \frac{1}{\sigma} \left[\int_0^{\frac{\pi}{2}} \frac{d\sigma}{d\theta_f} d\theta_f - \int_{\frac{\pi}{2}}^{\pi} \frac{d\sigma}{d\theta_f} d\theta_f \right] \equiv \frac{\sigma(\cos \theta_f > 0) - \sigma(\cos \theta_f < 0)}{\sigma(\cos \theta_f > 0) + \sigma(\cos \theta_f < 0)} \\
= & \frac{3\alpha p_z}{4},
\end{aligned}$$

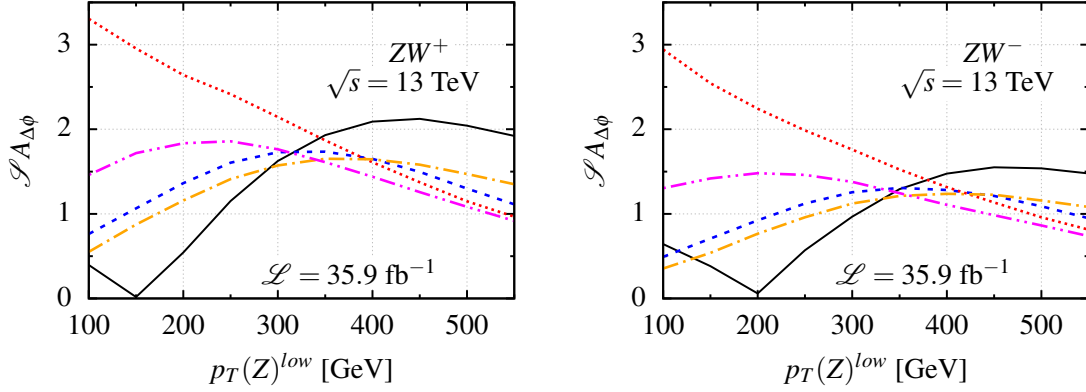


Figure 5: The sensitivity of the asymmetry $A_{\Delta\phi}$ on the five benchmark aTGC as a function of the lower cut on $p_T(Z)$ in the ZW^\pm production at the LHC at $\sqrt{s} = 13$ TeV and $\mathcal{L} = 35.9$ fb $^{-1}$. The legend labels are same as in Fig. 4.

$$\begin{aligned}
A_{xz} &= \frac{1}{\sigma} \left[\left(\int_{\theta=0}^{\frac{\pi}{2}} \int_{\phi=-\frac{\pi}{2}}^{\frac{\pi}{2}} \frac{d\sigma}{d\Omega_f} d\Omega_f + \int_{\theta=\frac{\pi}{2}}^{\pi} \int_{\phi=\frac{\pi}{2}}^{\frac{3\pi}{2}} \frac{d\sigma}{d\Omega_f} d\Omega_f \right) \right. \\
&\quad \left. - \left(\int_{\theta=0}^{\frac{\pi}{2}} \int_{\phi=\frac{\pi}{2}}^{\frac{3\pi}{2}} \frac{d\sigma}{d\Omega_f} d\Omega_f + \int_{\theta=\frac{\pi}{2}}^{\pi} \int_{\phi=-\frac{\pi}{2}}^{\frac{\pi}{2}} \frac{d\sigma}{d\Omega_f} d\Omega_f \right) \right] \\
&\equiv \frac{\sigma(\cos \theta_f \cos \phi_f > 0) - \sigma(\cos \theta_f \cos \phi_f < 0)}{\sigma(\cos \theta_f \cos \phi_f > 0) + \sigma(\cos \theta_f \cos \phi_f < 0)} \\
&= \frac{2}{\pi} \sqrt{\frac{2}{3}} (1 - 3\delta) T_{xz} .
\end{aligned} \tag{3.2}$$

Similarly one can construct asymmetries corresponding to each of the other polarizations p_i and T_{ij} ; see Ref. [80] for details.

The Z and the W^\pm bosons produced in the ZW^\pm production are not forward-backward symmetric owing to only a t -channel diagram and not having an u -channel diagram (see Fig. 1). These provide an extra observable, the forward-backward asymmetry defined as

$$A_{fb}^V = \frac{\sigma(\cos \theta_V > 0) - \sigma(\cos \theta_V < 0)}{\sigma(\cos \theta_V > 0) + \sigma(\cos \theta_V < 0)} , \tag{3.3}$$

θ_V is the production angle of the V w.r.t. the colliding quark-direction. One more angular variable sensitive to aTGC is the angular separation of the lepton l_W from W^\pm and the Z in the transverse plane, i.e.,

$$\Delta\phi(l_W, Z) = \cos^{-1} \left(\frac{\vec{p}_T(l_W) \cdot \vec{p}_T(Z)}{p_T(l_W) p_T(Z)} \right) . \tag{3.4}$$

One can construct an asymmetry based on the $\Delta\phi$ as,

$$A_{\Delta\phi} = \frac{\sigma(\cos(\Delta\phi(l_W, Z)) > 0) - \sigma(\cos(\Delta\phi(l_W, Z)) < 0)}{\sigma(\cos(\Delta\phi(l_W, Z)) > 0) + \sigma(\cos(\Delta\phi(l_W, Z)) < 0)} . \tag{3.5}$$

The sensitivities of $A_{\Delta\phi}$ to the five benchmark aTGC are shown in Fig. 5 as a function of lower cuts on $p_T(Z)$ in both ZW^\pm for luminosity of $\mathcal{L} = 35.9$ fb $^{-1}$. A choice of $p_T(Z)^{low} = 300$ GeV

appears to be an optimal choice for sensitivity for all the couplings. The m_{3l} cut, however, reduces the sensitivities to all the aTGC.

To construct the asymmetries, we need to set a reference frame and assign the leptons to the correct mother spin-1 particle. For the present process with missing neutrino, we face a set of challenges in constructing the asymmetries. These are discussed below.

Selecting Z candidate leptons The Z boson momentum is required to be reconstructed to obtain all the asymmetries which require the right pairing of the Z boson leptons l_Z^+ and l_Z^- . Although the opposite flavor channels $e^+e^-\mu^\pm/\mu^+\mu^-e^\pm$ are safe, the same flavor channels $e^+e^-e^\pm/\mu^+\mu^-\mu^\pm$ suffer ambiguity to select the right Z boson candidate leptons. The right pairing of leptons for the Z boson in the same flavored channel is possible with $\geq 96.5\%$ accuracy for $m_{3l} > 100$ GeV and $\geq 99.8\%$ accuracy for $m_{3l} > 550$ GeV in both SM and benchmark aTGC by requiring a smaller value of $|m_Z - m_{l+l-}|$. This small miss pairing is neglected to use the $2e\mu\nu_\mu$ channel as a proxy for a $3l + \cancel{E}_T$ final state with good enough accuracy.

The reconstruction of neutrino momentum The other major issue is to obtain the asymmetries related to W^\pm bosons, which require to reconstruct their momenta. As the neutrino from W^\pm goes missing, reconstruction of W^\pm boson momenta is possible with a two-fold ambiguity using the transverse missing energy p_T/\cancel{E}_T and the on-shell W mass (m_W) constrain. The two solutions for the longitudinal momentum of the missing neutrino are given by

$$p_z(\nu)_\pm = \frac{-\beta p_z(l_W) \pm E(l_W)\sqrt{D}}{p_T^2(l_W)} \quad (3.6)$$

with

$$D = \beta^2 - p_T^2(\nu)p_T^2(l_W), \quad \beta = m_W^2 + p_x(l_W)p_x(\nu) + p_y(l_W)p_y(\nu). \quad (3.7)$$

Because the W is not produced on-shell all the time, among the two solutions of longitudinal neutrino momenta, one of them will be closer to the true value, and another will be far from the true value. There are no suitable selector or discriminator to select the correct solution from the two solutions. Even if we substitute the Monte-Carlo truth m_W to solve for $p_z(\nu)$, we don't have any discriminator to distinguish between the two solutions $p_z(\nu)_\pm$. The smaller value of $|p_z(\nu)|$ corresponds to the correct solution only for $\approx 65\%$ times on average in ZW^+ and little lower in ZW^- production. One more discriminator, which is $||\beta_Z| - |\beta_W||$, the smaller value of this can choose the correct solution a little over the boundary, i.e., $\approx 55\%$. We have tried machine-learning approaches (artificial neural network) to select the correct solutions, but the accuracy was not better than 65%. In some cases, we have $D < 0$ with the on-shell W. For these cases, either one can throw those events (which affects the distribution and statistics), or one can vary the m_W from its central value to have $D > 0$. Here, we follow the latter. So, as the best available option, we choose the smaller value of $|p_z(\nu)|$ to be the correct solution to reconstruct the W boson momenta. At this point, it becomes important to explore the effect of reconstruction on asymmetries and their sensitivities to aTGC. To this end, we consider three scenarios:

Abs. True The first thing is to use the Monte-Carlo truth events and estimate the asymmetries in the lab frame. The observables in this scenario are directly related to the dynamics up to a rotation of frame [76, 108, 109].

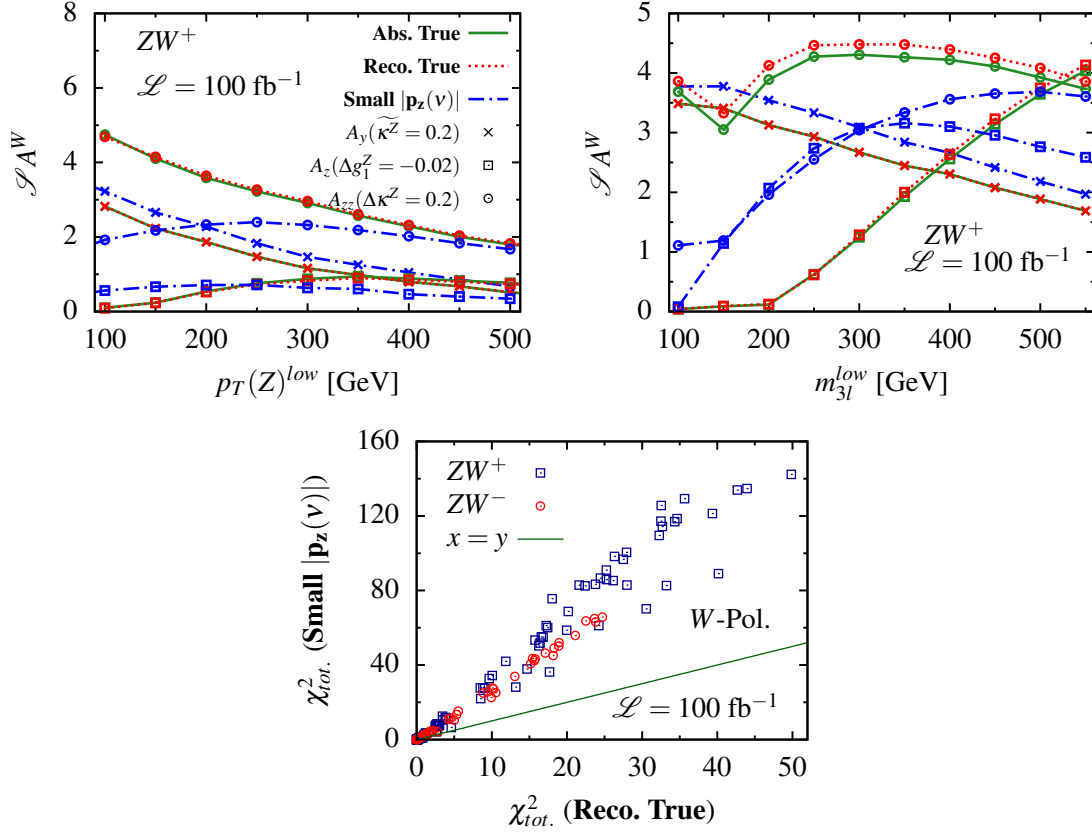


Figure 6: The sensitivity of some polarization asymmetries of W^+ (ZW^+) on some benchmark aTGC for three scenarios: with absolute truth (**Abs. True**) information of neutrino in *solid*/blue lines, with the close to true reconstructed solution of neutrino (**Reco. True**) in *dotted*/red lines and with the smaller $|\mathbf{p}_z(\nu)|$ to be the true solution (**Small $|\mathbf{p}_z(\nu)|$**) in *dash-dotted*/blue lines as a function of the lower cut on $p_T(Z)$ (*top-left-panel*) and m_{3l} (*top-right-panel*) at $\sqrt{s} = 13 \text{ TeV}$ and $\mathcal{L} = 100 \text{ fb}^{-1}$. The scatter plot of the total χ^2 for about 100 aTGC points using all the asymmetries of W^\pm for **Reco. True** in x -axis with **Small $|\mathbf{p}_z(\nu)|$** in y -axis is shown in the *bottom-panel*.

Reco. True Using the pole mass of W in Eq. (3.7) and choosing the solution closer to the Monte-Carlo true value is the best that one can do in reconstruction. The goal of any reconstruction algorithm would be to become as close to this scenario as possible.

Small $|\mathbf{p}_z(\nu)|$ This choice is the best available realistic algorithm which we will be using for the analysis.

The values of reconstructed asymmetries and hence polarizations get shifted from **Abs. True** case. In the case of **Reco. True**, the shifts are roughly constant, while in the case of **Small $|\mathbf{p}_z(\nu)|$** , the shifts are not constant over varying lower cuts on m_{3l} and $p_T(Z)$ due to the 35 % wrong choice. It is, thus, expected that the reconstructed sensitivities to aTGC remain the same in **Reco. True** and change in the **Small $|\mathbf{p}_z(\nu)|$** case when compared to the **Abs. True** case. In the **Small $|\mathbf{p}_z(\nu)|$** reconstruction case, sensitivities of some asymmetries to aTGC are less than that of the **Abs. True**

case, while they are higher for some other asymmetries. This is illustrated in Fig. 6 (*top-row*) comparing the sensitivity of some polarization asymmetries of W^+ , e.g., A_y to $\widetilde{\kappa^Z} = +0.2$ in cross (\times) points, A_z to $\Delta g_1^Z = -0.02$ in square (\square) points, and A_{zz} to $\Delta \kappa^Z = +0.2$ in circular (\odot) points for the three scenarios of **Abs. True** (*solid/blue line*), **Reco. True** (*dotted/red*) and **Small $|\mathbf{p}_z(\nu)|$** (*dash-dotted/blue*) for varying lower cuts on $p_T(Z)$ and m_{3l} in ZW^+ production with a luminosity of $\mathcal{L} = 100 \text{ fb}^{-1}$. The sensitivities are roughly the same for **Abs. True** and **Reco. True** reconstruction in all the asymmetries for both $p_T(Z)$ and m_{3l} cuts. In the **Small $|\mathbf{p}_z(\nu)|$** reconstruction case, sensitivity is smaller for A_{zz} , higher for A_y , and it depends on cut for A_z when compared to the **Abs. True** case. When all the W asymmetries are combined, the total χ^2 is higher in the **Small $|\mathbf{p}_z(\nu)|$** case compared to the **Reco. True** case for about 100 chosen benchmark points; see Fig. 6 (*bottom-panel*). Here, a total χ^2 of all the asymmetries of W (A_i^W) for a set of benchmark points ($\{c_i\}$) is given by

$$\chi^2(A_i^W)(\{c_i\}) = \sum_j^{N=9} (\mathcal{S}A_j^W(\{c_i\}))^2. \quad (3.8)$$

The said increment of χ^2 is observed in both W^+Z (\square /blue) and W^-Z (\odot /red) production processes. So even if we are not able to reconstruct the W and hence its polarization observables correctly, realistic effects end up enhancing the overall sensitivity of the observables to the aTGC.

Reference z -axis for polarizations The other challenge to obtain the polarization of V is that one needs a reference axis (z -axis) to get the momentum direction of V , which is not possible at the LHC as it is a symmetric collider. Thus, for the asymmetries related to Z boson, we consider the direction of total visible longitudinal momenta as an unambiguous choice for positive z -axis. For the case of W , the direction of the reconstructed boost is used as a proxy for the positive z -axis. The latter choice is inspired by the fact that in $q'\bar{q}$ fusion the quark is supposed to have larger momentum than the anti-quark at the LHC, thus the above proxy could stand statistically for the direction of the quark direction.

List of observables The set of observables used in this analysis are,

σ_i : The cross sections in four bins (4),

A_{pol}^Z : Eight polarization asymmetries of Z (8),

A_{fb}^Z : Forward-backward asymmetry of Z (1),

$A_{\Delta\phi}$: Azimuthal asymmetry (1),

A_{pol}^W : Eight polarization asymmetries of reconstructed W (8),

A_{fb}^W : Forward-backward asymmetry of reconstructed W ² (1),

which make a total of $N(\mathcal{O}) = (4 + 8 + 1 + 1 + 8 + 1) \times 2 = 46$ observables including both processes. All the asymmetry from Z side and all the asymmetries from W side are termed as A_i^Z and A_i^W ,

²We note that the forward-backward asymmetry of Z and W are ideally the same in the CM frame. However, since we measure the Z and $W \cos \theta$ w.r.t. different quantity, i.e., visible p_z for Z and reconstructed boost for W , they are practically different and we use them as two independent observables.

respectively, for the latter uses. The total χ^2 for all observables would be the quadratic sum of sensitivities (Eq. (2.3)) given by

$$\chi_{tot}^2(c_i) = \sum_j^{N=46} (\mathcal{S} \mathcal{O}_j(c_i))^2 . \quad (3.9)$$

We use these set of observables in some chosen kinematical region to obtain limits on aTGC in the next section.

4 Measurement of the anomalous couplings

We study the sensitivity of all the ($N(\mathcal{O}) = 46$) observables for varying lower cuts on m_{3l} and $p_T(Z)$ separately as well as simultaneously (grid scan in step of 50 GeV in each direction) for the chosen benchmark anomalous couplings. The maximum sensitivities are observed for simultaneous lower cuts on m_{3l} and $p_T(Z)$ given in Table 4 for all the asymmetries in both ZW^\pm processes. Some of these cuts can be realised from Fig. 5 & 6. The SM values of the asymmetries of Z and W and their corresponding polarizations for the selection cuts (sel.cut in Eq. (2.2)) and for the optimized cuts (opt.cut in Table 4) are listed in Table 6 in appendix B for completeness. We use the cross sections in the four bins and all the asymmetries with the optimized cuts to obtain limits on the anomalous couplings for both effective vertices and effective operators. We use the semi-analytical expressions for the observables fitted with the simulated data from mg5_aMC. The details of the fitting procedures are described in appendix A. The uncertainty on the cross sections and asymmetries are taken as $\varepsilon_\sigma = 20\%$ and $\varepsilon_A = 2\%$, respectively consistent with the analysis by CMS [98] and ATLAS [94]. We note that these uncertainties are not considered in the previous sections for qualitative analysis and optimization of cuts.

The sensitivities of all the observables to the aTGC are studied by varying one-parameter, two-parameter, and all-parameter at a time in the optimized cut region. We look at the $\chi^2 = 4$ contours in the $\Delta\kappa^Z\text{-}\widetilde{\kappa}^Z$ plane for a luminosity of $\mathcal{L} = 100 \text{ fb}^{-1}$ for various combinations of asymmetries and cross sections and show them in Fig. 7. We observe that the Z -asymmetries (A_i^Z) are weaker than the W -asymmetries (A_i^W); A_i^W provides very symmetric limits, while A_i^Z has a sense of directionality. The $A_{\Delta\phi}$ is better than both A_i^Z and A_i^W in most of the directions in $\Delta\kappa^Z\text{-}\widetilde{\kappa}^Z$ plane. After combining A_i^Z , A_i^W and $A_{\Delta\phi}$, we get a tighter contours; but the shape is dictated by $A_{\Delta\phi}$. We see (Fig. 7 *right-panel*) that the cross sections have higher sensitivity compared to the asymmetries to the aTGC. The cross sections dominate constraining the couplings, while the contribution from the asymmetries remain sub-dominant at best. Although the directional constraints provided by the asymmetries get washed away when combined with the cross sections, they are expected to remain prominent to extract *non-zero* couplings should a deviation from the SM be observed. This possibility is discussed in subsection 4.2.

4.1 Limits on the couplings

We extract simultaneous limits on all the anomalous couplings using all the observables using the MCMC method. We perform this analysis in two ways: (i) vary effective vertex factors couplings ($c_i^{\mathcal{L}}$) and (ii) vary effective operators couplings ($c_i^{\mathcal{O}}$) and translate them in to effective vertex factors

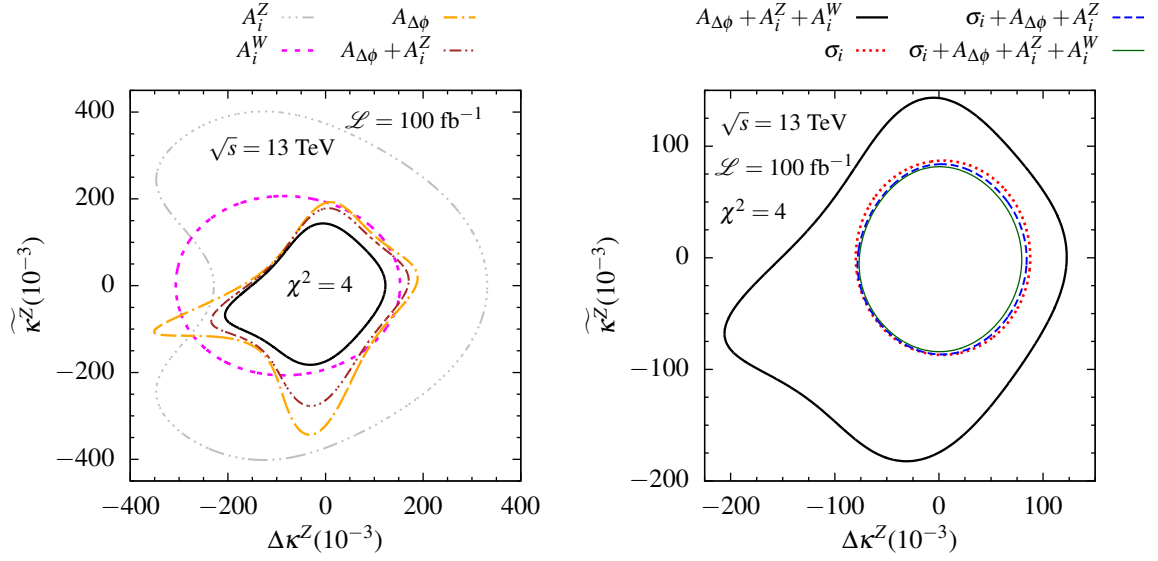


Figure 7: The $\chi^2 = 4$ contours are shown in the $\Delta\kappa^Z - \widetilde{\kappa^Z}$ plane with different asymmetries and their combinations in the *left-panel*, various combinations of the cross sections and asymmetries in the *right-panel* for $\sqrt{s} = 13$ TeV and $\mathcal{L} = 100 \text{ fb}^{-1}$. The contour for $A_{\Delta\phi} + A_i^Z + A_i^W$ (thick-solid/black line) is repeated in both *panel* for comparison.

Table 4: The list of optimized lower cuts (opt. cut) in GeV on $(m_{3l}, p_T(Z))$ for various asymmetries to maximize their sensitivity to the anomalous couplings.

\mathcal{O}	Z in ZW^+	Z in ZW^-	W^\pm in ZW^\pm
A_x	(200, 100)	(100, 150)	(250, 0)
A_y	(150, 100)	(100, 100)	''
A_z	(550, 50)	(100, 250)	''
A_{xy}	(150, 100)	(150, 100)	''
A_{xz}	(150, 0)	(200, 50)	''
A_{yz}	(100, 50)	(100, 0)	''
$A_{x^2-y^2}$	(400, 150)	(300, 100)	''
A_{zz}	(550, 0)	(300, 400)	''
A_{fb}	(300, 0)	(550, 0)	''
ZW^+		ZW^-	
$A_{\Delta\phi}$	(100, 300)	(100, 300)	

Table 5: The list of simultaneous limits from the MCMC at 95 % BCI on the effective vertex couplings $c_i^{\mathcal{L}}$ and the effective operator couplings $c_i^{\mathcal{O}}$ along with translated limits on effective vertices $c_i^{\mathcal{L}^g}$ for various luminosities with the notation $c_i^{\mathcal{L}^g} \equiv [lower\ limit, higher\ limit]$.

$c_i^{\mathcal{L}} (10^{-3})$	35.9 fb ⁻¹	100 fb ⁻¹	300 fb ⁻¹	1000 fb ⁻¹	3000 fb ⁻¹
Δg_1^Z	+2.15 -4.20	+1.50 -3.47	+0.963 -2.92	+0.565 -2.48	+0.318 -2.17
λ^Z	+2.11 -2.24	+1.66 -1.78	+1.30 -1.42	+1.01 -1.14	+0.811 -0.931
$\Delta \kappa^Z$	+83.5 -83.0	+66.6 -64.1	+52.8 -47.9	+42.1 -34.2	+36.0 -27.2
$\widetilde{\lambda}^Z$	+2.19 -2.19	+1.72 -1.74	+1.36 -1.38	+1.09 -1.09	+0.883 -0.884
$\widetilde{\kappa}^Z$	+86.2 -88.4	+67.5 -70.4	+51.8 -54.9	+40.1 -43.2	+33.9 -36.7
$c_i^{\mathcal{O}} (\text{TeV}^{-2})$					
$\frac{c_{WWWW}}{\Lambda^2}$	+0.540 -0.565	+0.426 -0.445	+0.327 -0.365	+0.257 -0.258	+0.200 -0.238
$\frac{c_W}{\Lambda^2}$	+0.504 -0.747	+0.397 -0.683	+0.274 -0.624	+0.196 -0.390	+0.138 -0.381
$\frac{c_B}{\Lambda^2}$	+67.8 -67.1	+60.1 -59.2	+47.6 -52.6	+30.9 -33.3	+27.0 -30.1
$\frac{c_{\widetilde{WWW}}}{\Lambda^2}$	+0.516 -0.514	+0.415 -0.430	+0.339 -0.342	+0.252 -0.244	+0.209 -0.216
$\frac{c_{\widetilde{W}}}{\Lambda^2}$	+69.2 -68.5	+61.2 -60.4	+52.7 -52.0	+34.2 -32.7	+31.0 -30.0
$c_i^{\mathcal{L}^g} (10^{-3})$					
Δg_1^Z	+2.10 -3.10	+1.65 -2.84	+1.14 -2.59	+0.814 -1.62	+0.576 -1.58
λ^Z	+2.21 -2.31	+1.74 -1.82	+1.34 -1.49	+1.05 -1.06	+0.822 -0.975
$\Delta \kappa^Z$	+62.1 -63.4	+54.6 -56.4	+48.3 -44.8	+30.6 -29.1	+27.6 -25.6
$\widetilde{\lambda}^Z$	+2.11 -2.10	+1.70 -1.76	+1.39 -1.40	+1.03 -1.00	+0.857 -0.882
$\widetilde{\kappa}^Z$	+63.8 -64.5	+56.3 -57.1	+48.4 -49.1	+30.5 -31.9	+28.0 -28.9

couplings ($c_i^{\mathcal{L}^g}$) using Eq. (1.4). The 95 % BCI (Bayesian confidence interval) obtained on aTGC are listed in Table 5 for five choices of integrated luminosities: $\mathcal{L} = 35.9 \text{ fb}^{-1}$, $\mathcal{L} = 100 \text{ fb}^{-1}$, $\mathcal{L} = 300 \text{ fb}^{-1}$, $\mathcal{L} = 1000 \text{ fb}^{-1}$ and $\mathcal{L} = 3000 \text{ fb}^{-1}$. The correlation among the parameters are studied (using GetDist [110]) and they are shown in Fig. 8 along with 1D projections for effective vertex factors. The limits on the couplings get tighter as the luminosity is increased, as it should be. The shape of the contours are very circular in all two-parameter projections as the cross sections dominate in constraining the aTGC. The same conclusions are drawn when effective operators are varied as independent parameters. The limits on $c_i^{\mathcal{L}^g}$ are tighter compared to the limits on $c_i^{\mathcal{L}}$ (see Table 5); the comparison between them are shown in the two-parameter marginalised plane in Fig. 9 in Δg_1^Z - κ^Z , λ^Z - $\widetilde{\lambda}^Z$ and κ^Z - $\widetilde{\kappa}^Z$ planes as representative for luminosity $\mathcal{L} = 100 \text{ fb}^{-1}$

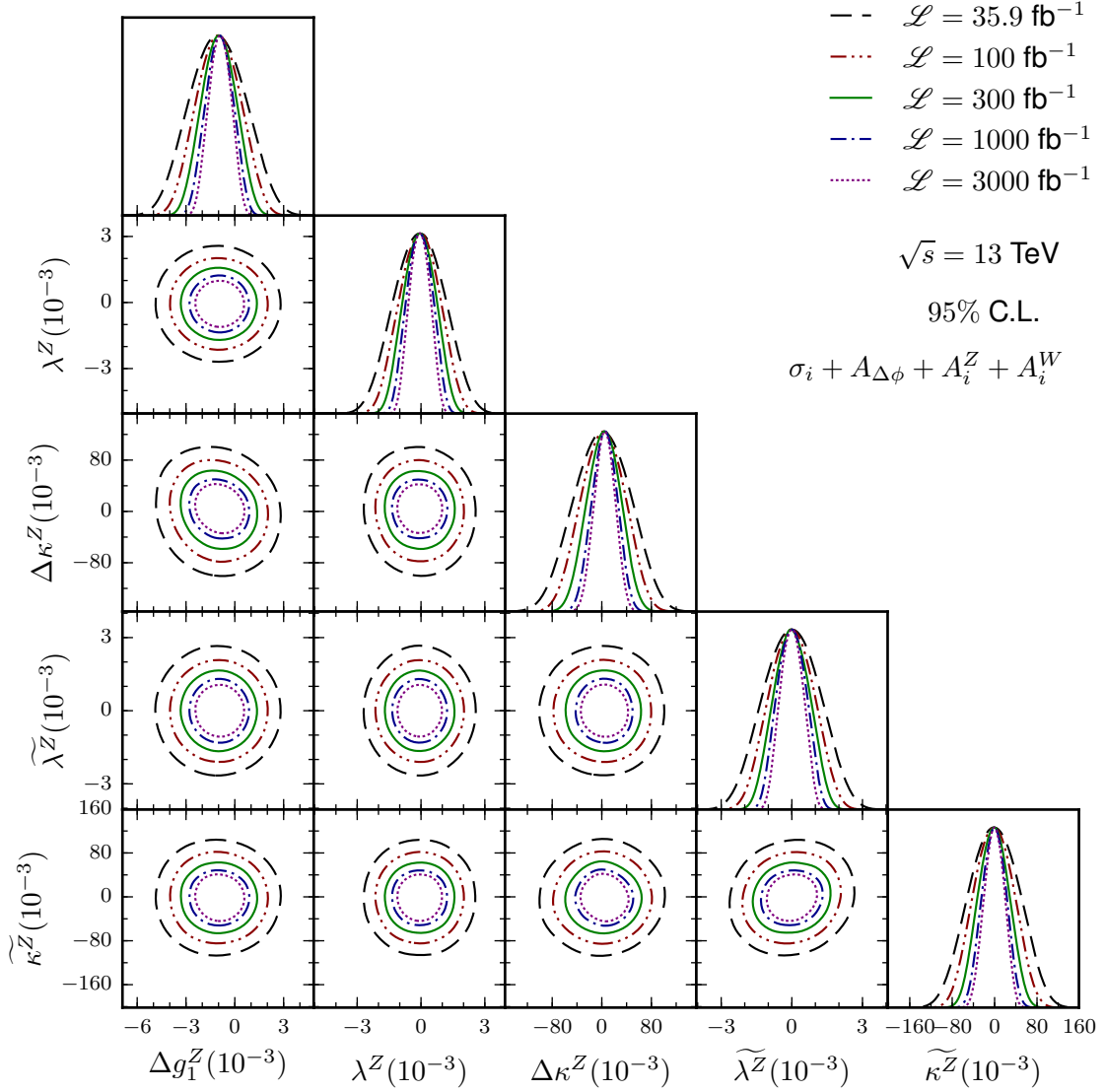


Figure 8: All the marginalised 1D projections and 2D projections at 95 % BCI from the MCMC in triangular array for the effective vertices ($c_i^{\mathcal{L}}$) for various luminosities at $\sqrt{s} = 13$ TeV using all the observables.

(outer contours) and $\mathcal{L} = 1000 \text{ fb}^{-1}$ (inner contours). The limits and the contours are roughly the same in λ^Z - $\tilde{\lambda}^Z$ plane. The contours are more symmetric around the SM for $c_i^{\mathcal{L}_s}$ compared to $c_i^{\mathcal{L}}$, e.g.; see Δg_1^Z - κ^Z plane. The limits obtained here for luminosity 35.9 fb^{-1} are better than the experimentally observed limits at the LHC given in Table 1 except on c_B and hence on $\Delta \kappa^Z$. This is because the LHC analysis [72] uses WW production on top of ZW production, whereas we only use ZW production process. But our limits on the couplings are better when compared with the ZW production process alone at the LHC [74]. In Fig. 10, we present the comparison of limits obtained by the CMS analyses with $ZW + WW$ [72] process and ZW [74] with our estimate with two parameter 95 % BCI contours in the c_{WW}/Λ^2 - c_W/Λ^2 plane (left-panel) and c_W/Λ^2 -

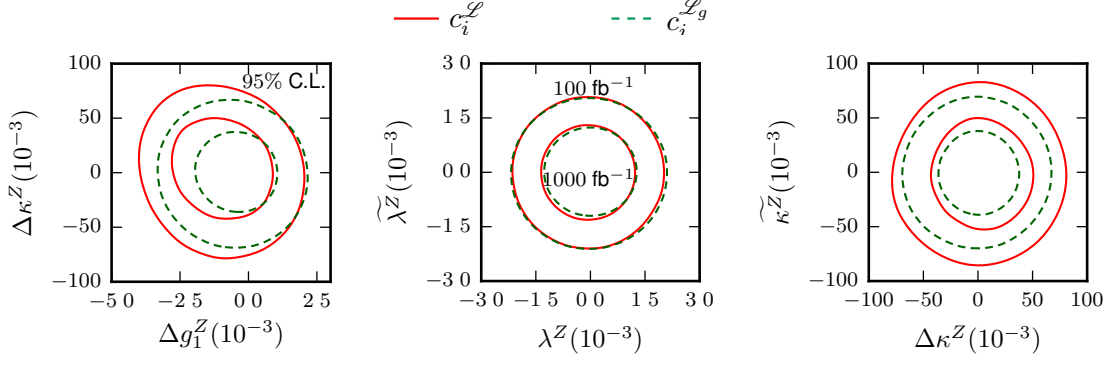


Figure 9: The marginalised 2D projections at 95 % BCI from the MCMC in the Δg_1^Z - $\Delta \kappa^Z$, λ^Z - λ^Z , and $\Delta \kappa^Z$ - κ^Z planes are shown in *solid/red* when the effective vertex factors ($c_i^{\mathcal{L}}$) are treated independent, while shown in *dashed/green* when the operators are treated independent ($c_i^{\mathcal{L}_g}$) for luminosities $\mathcal{L} = 1000 \text{ fb}^{-1}$ (two inner contours) and $\mathcal{L} = 100 \text{ fb}^{-1}$ (two outer contours) at $\sqrt{s} = 13 \text{ TeV}$ using all the observables.

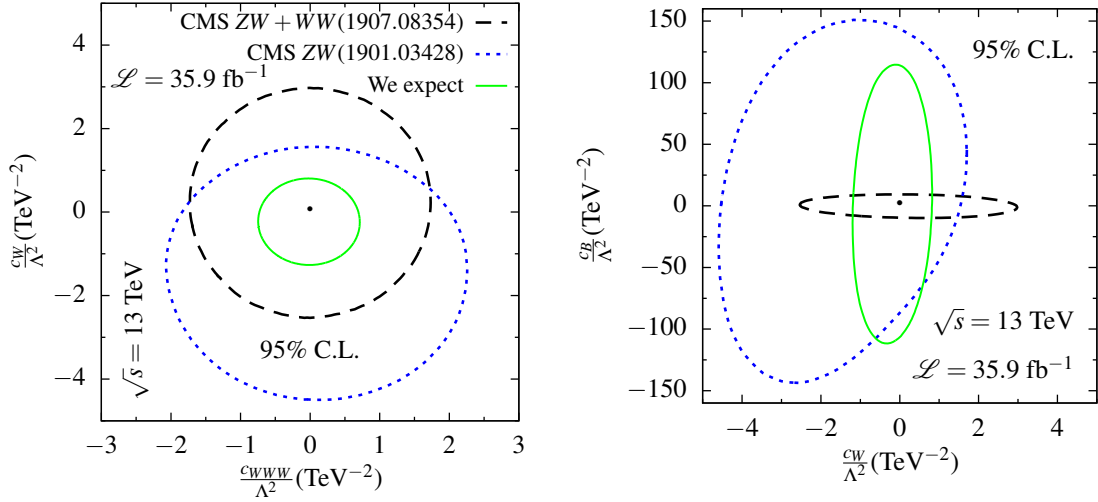


Figure 10: The two parameter 95 % C.L. contours in the c_{WWW}/Λ^2 - c_W/Λ^2 plane (*left-panel*) and c_W/Λ^2 - c_B/Λ^2 plane (*right-panel*) for our estimate (We expect) in *solid/green* lines, for CMS ZW + WW in *dashed/black* lines and for CMS ZW in *dotted/blue* lines at $\sqrt{s} = 13 \text{ TeV}$ and $\mathcal{L} = 35.9 \text{ fb}^{-1}$ using all the observables.

c_B/Λ^2 plane (*right-panel*). The contour in the plane c_{WWW}/Λ^2 - c_W/Λ^2 in our estimate (We expect) (*solid/green* line) is tighter compared to both CMS ZW + WW (*dashed/black* line) and CMS ZW analyses (*dotted/blue* line). This is because we use binned cross sections in the analysis. The limit on the couplings c_B/Λ^2 (*right-panel*) on the other hand is tighter, yet comparable, with CMS ZW and weaker than the CMS ZW + WW analysis because the ZW process itself is less sensitive to c_W .

4.2 The role of asymmetries in parameter extraction

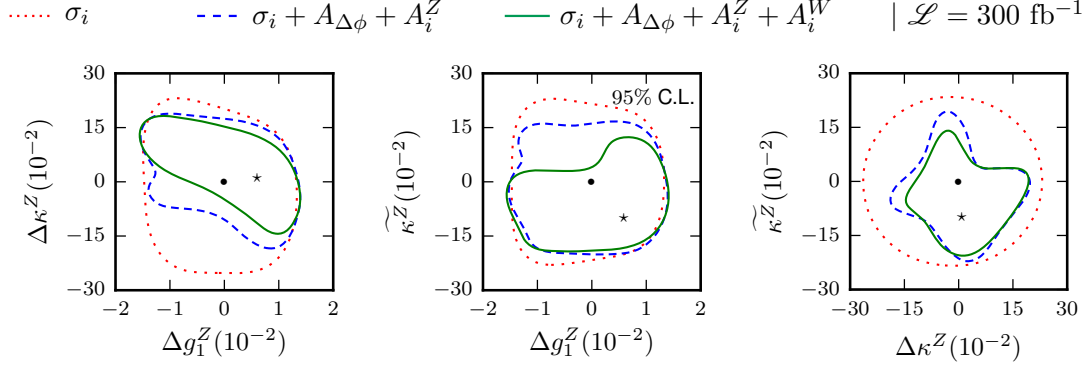


Figure 11: The marginalised 2D projections at 95 % BCI on Δg_1^Z - $\Delta \kappa^Z$, Δg_1^Z - $\widetilde{\kappa}^Z$, and $\Delta \kappa^Z$ - $\widetilde{\kappa}^Z$ planes from the MCMC with observables σ_i (dotted/red line), $\sigma_i + A_{\Delta\phi} + A_i^Z$ (dashed/blue line) and $\sigma_i + A_{\Delta\phi} + A_i^Z + A_i^W$ (solid/green line) for aTGC-Bench couplings $\{\Delta g_1^Z, \lambda^Z, \Delta \kappa^Z, \widetilde{\lambda}^Z, \widetilde{\kappa}^Z\} = \{0.6, 0.6, 0.8, 0.4, -10\} \times 10^{-2}$ at $\sqrt{s} = 13$ TeV and $\mathcal{L} = 300 \text{ fb}^{-1}$.

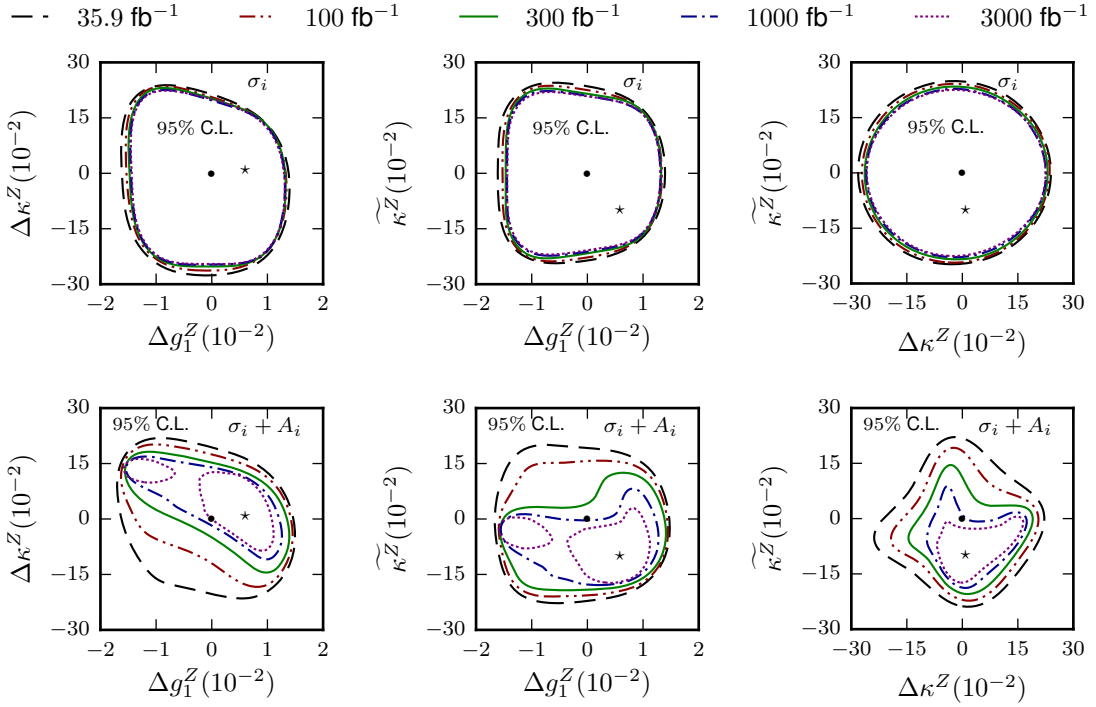


Figure 12: The marginalised 2D projections at 95 % BCI on Δg_1^Z - $\Delta \kappa^Z$, Δg_1^Z - $\widetilde{\kappa}^Z$, and $\Delta \kappa^Z$ - $\widetilde{\kappa}^Z$ planes from the MCMC with observables σ_i in *top-row* and $\sigma_i + A_{\Delta\phi} + A_i^Z + A_i^W$ in *bottom-row* for integrated luminosities 35.9 fb^{-1} (outermost contours), 100 fb^{-1} , 300 fb^{-1} , 1000 fb^{-1} , and 3000 fb^{-1} (innermost contours) for aTGC-Bench couplings $\{\Delta g_1^Z, \lambda^Z, \Delta \kappa^Z, \widetilde{\lambda}^Z, \widetilde{\kappa}^Z\} = \{0.6, 0.6, 0.8, 0.4, -10\} \times 10^{-2}$ at $\sqrt{s} = 13$ TeV.

The asymmetries are sub-dominant in constraining the couplings much like seen in Ref. [90]

for $pp \rightarrow ZZ$ case. But the asymmetries have a sense of directionality in the parameter space. To see this, we perform a toy analysis to extract *non-zero* anomalous couplings with pseudo data generated for the set of anomalous couplings of

$$\text{aTGC-Bench} : \{\Delta g_1^Z, \lambda^Z, \Delta \kappa^Z, \widetilde{\lambda}^Z, \widetilde{\kappa}^Z\} = \{0.6, 0.6, 0.8, 0.4, -10\} \times 10^{-2} \quad (4.1)$$

using the MCMC method. These couplings are chosen to be within the current limits; see Table 1. In Fig. 11, we show the posterior marginalised 2D projections at 95 % BCI on $\Delta g_1^Z - \Delta \kappa^Z$, $\Delta g_1^Z - \widetilde{\kappa}^Z$, and $\Delta \kappa^Z - \widetilde{\kappa}^Z$ planes. We draw the contours using σ_i only (*dotted/red* line), using σ_i along with $A_{\Delta\phi} + A_i^Z$ (*dashed/blue* line) and all observables $\sigma_i + A_{\Delta\phi} + A_i^Z + A_i^W$ (*solid/green* line) for integrated luminosity of $\mathcal{L} = 300 \text{ fb}^{-1}$. The dot (\bullet) points in the 2D contours represent the SM point, while the star-marks (\star) represent the couplings from aTGC-Bench. As the asymmetries $A_{\Delta\phi}$ and asymmetries of Z (A_i^Z) are added on top of the cross sections, the measurement gets better and it improves further when the asymmetries of W (A_i^W) are added. The cross sections are blind to the orientation of aTGC-Bench couplings and sensitive only to the magnitude of deviation from the SM. The asymmetries, however, give direction to the measurement, e.g., in $\Delta \kappa^Z - \widetilde{\kappa}^Z$ plane, $\sigma_i + A_{\Delta\phi} + A_i^Z$ give tight and directional constraints. The above three planes are shown again in Fig. 12 for varying luminosities of 35.9 fb^{-1} (outermost contours), 100 fb^{-1} , 300 fb^{-1} , 1000 fb^{-1} , and 3000 fb^{-1} (innermost contours) for observables σ_i in *top-row* and $\sigma_i + A_{\Delta\phi} + A_i^Z$ in *bottom-row*. For higher luminosities, the σ_i alone (*top-row*) do not yield improved limits nor do they give any hint towards the direction of aTGC-Bench. But the inclusion of asymmetries $\sigma_i + A_i$ (*bottom-row*) give increasingly accurate determination of the aTGC-Bench points with increasing luminosity. Thus, this toy analysis indicates that the asymmetries would help in the measurement of anomalous couplings at high-luminosity provided an excess of events is observed at the LHC, and we interpret the deviation in terms of aTGC.

We note that the $3l + \cancel{E}_T$ excess in the lower $p_T(Z)$ region at the LHC [74] interpreted by two extra scalar[111] may be fitted by aTGC, which is beyond the scope of this present work.

5 Conclusion

To conclude, we studied the WWZ anomalous couplings in the ZW^\pm production at the LHC and examined the role of polarization asymmetries together with $\Delta\phi(l_W, Z)$ asymmetry and forward-backward asymmetry on the estimation of limits on the anomalous couplings. We reconstructed the missing neutrino momentum by choosing the small $|p_z(\nu)|$ from the two-fold solutions and estimated the W polarization asymmetries, while the Z polarization asymmetries are kept free from any reconstruction ambiguity. We generated events at NLO in QCD in mg5_aMC for about 100 sets of anomalous couplings and used them for the numerical fitting of semi-analytic expressions of all the observables as a function of the couplings. We estimated simultaneous limits on the anomalous couplings using the MCMC method for both the effective vertex formalism and the effective operator approach for luminosities 35.9 fb^{-1} , 100 fb^{-1} , 300 fb^{-1} , 1000 fb^{-1} , and 3000 fb^{-1} . The limits obtained for $\mathcal{L} = 35.9 \text{ fb}^{-1}$ are tighter than the limits available at the LHC (see Table 1 & 5) except on c_W (and $\Delta \kappa^Z$). The asymmetries are helpful in extracting the values of anomalous couplings if a deviation from the SM is observed at the LHC. We performed a toy analysis of parameter extraction

with some benchmark aTGC couplings and observed that the inclusion of asymmetries to the cross sections improves the parameter extraction significantly at high-luminosity.

Acknowledgements: R.R. thanks Department of Science and Technology, Government of India for support through DST-INSPIRE Fellowship for doctoral program, INSPIRE CODE IF140075, 2014. RKS acknowledges SERB, DST, Government of India through the project EMR/2017/002778. The authors thank the anonymous referee for his/her suggestions for the improvement of this article.

A Fitting procedure in obtaining observables as a function of couplings

The SM+aTGC events are generated for about 100 set of couplings

$$\{c_i\} = \{\Delta g_1^Z, \lambda^Z, \Delta \kappa^Z, \widetilde{\lambda}^Z, \widetilde{\kappa}^Z\}$$

in both processes. The values of all the observables are obtained for the set couplings in the optimized cuts (Table 4), and then those are used for numerical fitting to obtain the semi-analytical expression of all the observables as a function of the couplings. For the cross sections the following CP -even expression is used to fit the data:

$$\sigma(\{c_i\}) = \sigma_{SM} + \sum_{i=1}^3 c_i \times \sigma_i + \sum_{i=1}^5 (c_i)^2 \times \sigma_{ii} + \frac{1}{2} \sum_{i=1}^3 \sum_{j(\neq i)=1}^3 c_i c_j \times \sigma_{ij} + c_4 c_5 \times \sigma_{45} . \quad (\text{A.1})$$

For asymmetries, the numerator and the denominator are fitted separately and then used as

$$A_j(\{c_i\}) = \frac{\Delta \sigma_{A_j}(\{c_i\})}{\sigma_{A_j}(\{c_i\})} . \quad (\text{A.2})$$

The numerator ($\Delta \sigma_A$) of CP -odd asymmetries are fitted with the CP -odd expression

$$\Delta \sigma_A(\{c_i\}) = \sum_{i=4}^5 c_i \times \sigma_i + \sum_{i=1}^3 (c_i c_4 \times \sigma_{i4} + c_i c_5 \times \sigma_{i5}) . \quad (\text{A.3})$$

The denominator (σ_{A_j}) of all the asymmetries and the numerator ($\Delta \sigma_A$) of CP -even asymmetries are fitted with the CP -even expression given in Eq. (A.1).

We use the MCMC method to fit the coefficients of the cross sections with positivity demand, i.e., $\sigma(\{c_i\}) \geq 0$. We use 80 % data to fit the coefficients of the cross sections, and then the fitted expressions are validated against the rest 20 % of the data and found to be matching within 2σ MC error. We generated 10^7 events to keep the MC error as small as possible, even in the tightest optimized cuts. For example, the A_{zz} in ZW^+ has the tightest cut on m_{3l} (see Table 4) and yet have very small (0.2 %) MC error (see Table 6). In Fig. 13 fitted values of observables are compared against the simulated data for the cross section in two diagonal bins (*top-panel*) and the polarization asymmetries A_z and A_{xz} (*bottom-panel*) in ZW^+ production in $e^+e^- \mu^+ \nu_\mu$ channel as representative. The fitted values seem to agree with the simulated data used within the MC error.

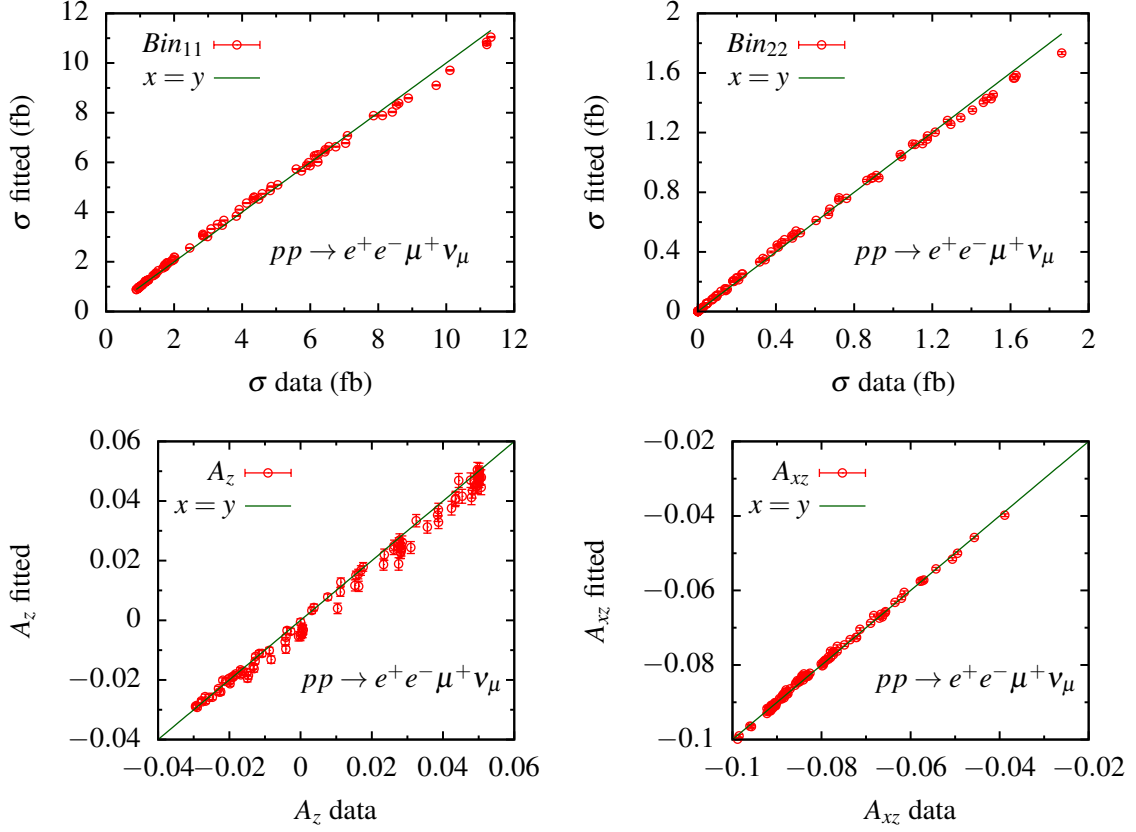


Figure 13: The simulated data (in x -axis) vs. fitted values (in y -axis) for the cross section in the two diagonal bins (*top-panel*) and the polarization asymmetries A_z and A_{xz} (*bottom-panel*) in ZW^+ production in $e^+e^-\mu^+\nu_\mu$ channel at the LHC at $\sqrt{s} = 13$ TeV.

Table 6: The SM values with 1σ MC error of the polarization asymmetries of Z and W and their corresponding polarizations along with the other asymmetries in ZW^\pm production in the $e^+e^-\mu^\pm+\cancel{E}_T$ channel are shown for event selection cuts (sel. cut) given in Eq. (2.2) and optimized cuts (opt. cut) given Table 4.

	ZW^+				ZW^-			
	Z		W^+		Z		W^-	
\mathcal{O}	sel. cut	opt. cut	sel. cut	opt. cut	sel. cut	opt. cut	sel. cut	opt. cut
δA_i	± 0.0003		± 0.0003	± 0.0007	± 0.0003		± 0.0003	± 0.0007
A_x	-0.0196	-0.0150 ± 0.0008	-0.2303	-0.0550	$+0.0074$	-0.0046 ± 0.0010	-0.0826	-0.0001
p_x	$+0.1192 \pm 0.0018$	$+0.0912 \pm 0.0049$	$+0.3071 \pm 0.0004$	0.0733 ± 0.0009	-0.0450 ± 0.0018	$+0.0280 \pm 0.0061$	$+0.110 \pm 0.00041$	$+0.00013 \pm 0.0009$
A_y	$+0.0003$	$+0.0004 \pm 0.0007$	-0.0007	-0.0005	-0.0013	-0.0021 ± 0.0007	0.0	$+0.0007$
p_y	-0.0018 ± 0.0018	-0.0024 ± 0.0146	$+0.0009 \pm 0.0004$	$+0.0006 \pm 0.0009$	$+0.0079 \pm 0.0018$	$+0.0127 \pm 0.0042$	0.0 ± 0.0004	-0.0009 ± 0.0009
A_z	-0.0040	$+0.0502 \pm 0.0025$	$+0.1337$	$+0.6615$	$+0.0316$	$+0.0482 \pm 0.0019$	$+0.1954$	$+0.7381$
p_z	$+0.0243 \pm 0.0018$	-0.3051 ± 0.0152	-0.1783 ± 0.0004	-0.8820 ± 0.0009	-0.1921 ± 0.0018	-0.2930 ± 0.0115	-0.2605 ± 0.0004	-0.9841 ± 0.0009
A_{xy}	-0.0017	$+0.0005 \pm 0.0007$	-0.0011	-0.0006	$+0.0008$	$+0.0014 \pm 0.0007$	$+0.0013$	-0.0003
T_{xy}	-0.0033 ± 0.0006	$+0.00096 \pm 0.0013$	-0.0021 ± 0.0006	-0.0012 ± 0.0013	$+0.0015 \pm 0.0006$	$+0.0027 \pm 0.0013$	$+0.0025 \pm 0.0006$	-0.0006 ± 0.0013
A_{xz}	$+0.0196$	$+0.0914 \pm 0.0004$	$+0.0048$	-0.0063	$+0.0961$	$+0.0547 \pm 0.0006$	$+0.0010$	-0.0136
T_{xz}	$+0.0377 \pm 0.0006$	$+0.1758 \pm 0.0008$	$+0.0092 \pm 0.0006$	-0.0121 ± 0.0013	$+0.1849 \pm 0.0006$	$+0.1052 \pm 0.0011$	$+0.0019 \pm 0.0006$	-0.0262 ± 0.0013
A_{yz}	$+0.0002$	-0.0001 ± 0.0004	$+0.0003$	-0.0005	-0.0017	-0.0016 ± 0.0003	$+0.0001$	-0.0001
T_{yz}	$+0.0004 \pm 0.0006$	-0.0002 ± 0.0008	$+0.0006 \pm 0.0006$	-0.0009 ± 0.0013	-0.0033 ± 0.0006	-0.0031 ± 0.0006	$+0.0002 \pm 0.0006$	-0.0002 ± 0.0013
$A_{x^2-y^2}$	-0.0878	-0.0925 ± 0.0019	-0.0266	-0.1326	-0.0935	-0.0899 ± 0.0012	-0.0923	-0.1588
$T_{xx}-T_{yy}$	-0.3378 ± 0.0011	-0.3559 ± 0.0073	-0.1023 ± 0.0011	-0.5102 ± 0.0027	-0.3597 ± 0.0011	-0.3459 ± 0.0046	-0.3551 ± 0.0011	-0.6110 ± 0.0027
A_{zz}	-0.0137	$+0.0982 \pm 0.0024$	$+0.0519$	$+0.1406$	$+0.0030$	$+0.0863 \pm 0.0048$	$+0.1046$	$+0.2547$
T_{zz}	-0.0298 ± 0.0006	$+0.2138 \pm .0052$	$+0.1130 \pm 0.0006$	$+0.3061 \pm 0.0015$	$+0.0065 \pm 0.0006$	$+0.1879 \pm 0.0104$	$+0.2277 \pm 0.0006$	$+0.5546 \pm 0.0015$
$A_{f/b}$	$+0.6829$	$+0.4475 \pm 0.0009$	$+0.4699$	$+0.2627$	$+0.6696$	$+0.2791 \pm 0.0025$	$+0.2060$	$+0.3174$
	sel. cut		opt. cut		sel. cut		opt. cut	
$A_{\Delta\phi}$	-0.3756 ± 0.0003		-0.4151 ± 0.0022		-0.3880 ± 0.0003		-0.4208 ± 0.0025	

B Standard Model values of the asymmetries and polarizations

In Table 6, we show the SM estimates (with 1σ MC error) of the polarization asymmetries of Z and W and their corresponding polarizations along with the other asymmetries for our selection cuts (`sel.cut`) given in Eq. (2.2) and optimized cuts (`opt.cut`) given Table 4. A number of events of $N \simeq 9.9 \times 10^6$ satisfy our selection cuts, which give the same error ($\delta A_i = 1/\sqrt{N}$) for all the asymmetries, and hence they are given in the top row. As the optimized cuts for W are the same for all the asymmetries, the errors for them are also given in the top row. For the optimized cuts of Z observables, however, the number of events varies, and hence the MC errors are given to each asymmetries. The CP -odd polarizations p_y , T_{xy} , T_{yz} , and their corresponding asymmetries are consistent with zero in the SM within MC error.

References

- [1] CMS Collaboration, S. Chatrchyan *et al.*, *Observation of a new boson at a mass of 125 GeV with the CMS experiment at the LHC*, *Phys. Lett. B* **716** (2012) 30–61, [arXiv:1207.7235 \[hep-ex\]](#).
- [2] ATLAS Collaboration, G. Aad *et al.*, *Observation of a new particle in the search for the Standard Model Higgs boson with the ATLAS detector at the LHC*, *Phys. Lett. B* **716** (2012) 1–29, [arXiv:1207.7214 \[hep-ex\]](#).
- [3] ATLAS Collaboration, *ATLAS Summary plot for exotics*, https://atlas.web.cern.ch/Atlas/GROUPS/PHYSICS/CombinedSummaryPlots/EXOTICS/ATLAS_Exotics_Summary/ATLAS_Exotics_Summary_201905.png, (May 2019).
- [4] ATLAS Collaboration, *ATLAS Summary plot for SUSY*, https://atlas.web.cern.ch/Atlas/GROUPS/PHYSICS/CombinedSummaryPlots/SUSY/ATLAS_SUSY_Summary/ATLAS_SUSY_Summary_201907.png, (July 2019).
- [5] CMS Collaboration, *CMS Summary plot for exotics*, https://twiki.cern.ch/twiki/pub/CMSPublic/SummaryPlotsEXO13TeV/EXO_barchart_Jan19.png, (January 2019).
- [6] CMS Collaboration, *CMS Summary plot for long lived particle*, https://twiki.cern.ch/twiki/pub/CMSPublic/SummaryPlotsEXO13TeV/CMS_LL_P_barchart.png, (July 2019).
- [7] CMS Collaboration, *CMS Summary plot for Beyond-two-generations (B2G)*, https://twiki.cern.ch/twiki/pub/CMSPublic/PhysicsResultsB2G/barplot_DIB_RES_VHF.png, (July 2019).
- [8] ATLAS Collaboration, M. Aaboud *et al.*, *Search for resonances in diphoton events at $\sqrt{s}=13$ TeV with the ATLAS detector*, *JHEP* **09** (2016) 001, [arXiv:1606.03833 \[hep-ex\]](#).
- [9] CMS Collaboration, V. Khachatryan *et al.*, *Search for Resonant Production of High-Mass Photon Pairs in Proton-Proton Collisions at $\sqrt{s}=8$ and 13 TeV*, *Phys. Rev. Lett.* **117** no. 5, (2016) 051802, [arXiv:1606.04093 \[hep-ex\]](#).
- [10] CMS Collaboration, A. M. Sirunyan *et al.*, *Search for resonances in the mass spectrum of muon pairs produced in association with b quark jets in proton-proton collisions at $\sqrt{s}=8$ and 13 TeV*, *JHEP* **11** (2018) 161, [arXiv:1808.01890 \[hep-ex\]](#).
- [11] K. Hagiwara, S. Ishihara, R. Szalapski, and D. Zeppenfeld, *Low-energy effects of new interactions in the electroweak boson sector*, *Phys. Rev. D* **48** (1993) 2182–2203.

- [12] C. Degrande, N. Greiner, W. Kilian, O. Mattelaer, H. Mebane, T. Stelzer, S. Willenbrock, and C. Zhang, *Effective Field Theory: A Modern Approach to Anomalous Couplings*, *Annals Phys.* **335** (2013) 21–32, [arXiv:1205.4231 \[hep-ph\]](#).
- [13] K. Hagiwara, R. D. Peccei, D. Zeppenfeld, and K. Hikasa, *Probing the Weak Boson Sector in $e^+e^- \rightarrow W^+W^-$* , *Nucl. Phys.* **B282** (1987) 253–307.
- [14] J. Wudka, *Electroweak effective Lagrangians*, *Int. J. Mod. Phys.* **A9** (1994) 2301–2362, [arXiv:hep-ph/9406205 \[hep-ph\]](#).
- [15] A. B. Lahanas and V. C. Spanos, *Static quantities of the W boson in the MSSM*, *Phys. Lett.* **B334** (1994) 378–390, [arXiv:hep-ph/9405298 \[hep-ph\]](#).
- [16] A. Arhrib, J. L. Kneur, and G. Moultaka, *Radiative contributions to TGC in the MSSM*, in *e^+e^- collisions at TeV energies: The physics potential. Proceedings, Workshop, Annecy, France, February 4, 1995, Gran Sasso, Assergi, Italy, June 2-3, 1995, Hamburg, Germany, August 30-September 1, 1995*, pp. 331–334. 1996. [arXiv:hep-ph/9603268 \[hep-ph\]](#). [,331(1996)].
- [17] E. N. Argyres, A. B. Lahanas, C. G. Papadopoulos, and V. C. Spanos, *Trilinear gauge boson couplings in the MSSM*, *Phys. Lett.* **B383** (1996) 63–77, [arXiv:hep-ph/9603362 \[hep-ph\]](#).
- [18] A. Flores-Tlalpa, J. Montano, H. Novales-Sanchez, F. Ramirez-Zavaleta, and J. J. Toscano, *One-loop effects of extra dimensions on the $WW\gamma$ and WWZ vertices*, *Phys. Rev.* **D83** (2011) 016011, [arXiv:1009.0063 \[hep-ph\]](#).
- [19] M. López-Osorio, E. Martínez-Pascual, J. Montaña, H. Novales-Sánchez, J. J. Toscano, and E. S. Tututi, *Trilinear gauge boson couplings in the standard model with one universal extra dimension*, *Phys. Rev.* **D88** no. 1, (2013) 016010, [arXiv:1305.0621 \[hep-ph\]](#).
- [20] M. A. Arroyo-Ureña, G. Hernández-Tomé, and G. Tavares-Velasco, *WWV ($V = \gamma, Z$) vertex in the Georgi-Machacek model*, *Phys. Rev.* **D94** no. 9, (2016) 095006, [arXiv:1610.04911 \[hep-ph\]](#).
- [21] E. N. Argyres, G. Katsilieris, A. B. Lahanas, C. G. Papadopoulos, and V. C. Spanos, *One loop corrections to three vector boson vertices in the Standard Model*, *Nucl. Phys.* **B391** (1993) 23–41.
- [22] J. Papavassiliou and K. Philippides, *Gauge invariant three boson vertices in the Standard Model and the static properties of the W*, *Phys. Rev.* **D48** (1993) 4255–4268, [arXiv:hep-ph/9310210 \[hep-ph\]](#).
- [23] K. J. F. Gaemers and G. J. Gounaris, *Polarization Amplitudes for $e^+e^- \rightarrow W^+W^-$ and $e^+e^- \rightarrow ZZ$* , *Z. Phys.* **C1** (1979) 259.
- [24] C. L. Bilchak and J. D. Stroughair, *W^+W^- Pair Production in e^+e^- Colliders*, *Phys. Rev.* **D30** (1984) 1881.
- [25] K. Hagiwara, S. Ishihara, R. Szalapski, and D. Zeppenfeld, *Low-energy constraints on electroweak three gauge boson couplings*, *Phys. Lett.* **B283** (1992) 353–359.
- [26] J. D. Wells and Z. Zhang, *Status and prospects of precision analyses with $e^+e^- \rightarrow W^+W^-$* , *Phys. Rev.* **D93** no. 3, (2016) 034001, [arXiv:1507.01594 \[hep-ph\]](#). [Phys. Rev.D93,034001(2016)].
- [27] G. Buchalla, O. Cata, R. Rahn, and M. Schlaffer, *Effective Field Theory Analysis of New Physics in $e^+e^- \rightarrow W^+W^-$ at a Linear Collider*, *Eur. Phys. J.* **C73** no. 10, (2013) 2589, [arXiv:1302.6481 \[hep-ph\]](#).
- [28] Z. Zhang, *Time to Go Beyond Triple-Gauge-Boson-Coupling Interpretation of W Pair Production*, *Phys. Rev. Lett.* **118** no. 1, (2017) 011803, [arXiv:1610.01618 \[hep-ph\]](#).

- [29] L. Berthier, M. Bjørn, and M. Trott, *Incorporating doubly resonant W^\pm data in a global fit of SMEFT parameters to lift flat directions*, *JHEP* **09** (2016) 157, [arXiv:1606.06693 \[hep-ph\]](#).
- [30] L. Bian, J. Shu, and Y. Zhang, *Prospects for Triple Gauge Coupling Measurements at Future Lepton Colliders and the 14 TeV LHC*, *JHEP* **09** (2015) 206, [arXiv:1507.02238 \[hep-ph\]](#).
- [31] L. Bian, J. Shu, and Y. Zhang, *Triple gauge couplings at future hadron and lepton colliders*, *Int. J. Mod. Phys. A* **31** no. 33, (2016) 1644008, [arXiv:1612.03888 \[hep-ph\]](#).
- [32] D. Choudhury and J. Kalinowski, *Unraveling the $WW\gamma$ and WWZ vertices at the linear collider: Anti-neutrino neutrino γ and anti-neutrino neutrino $\bar{q}q$ final states*, *Nucl. Phys. B* **491** (1997) 129–146, [arXiv:hep-ph/9608416 \[hep-ph\]](#).
- [33] D. Choudhury, J. Kalinowski, and A. Kulesza, *CP violating anomalous $WW\gamma$ couplings in e^+e^- collisions*, *Phys. Lett. B* **457** (1999) 193–201, [arXiv:hep-ph/9904215 \[hep-ph\]](#).
- [34] R. Rahaman and R. K. Singh, *Probing the anomalous triple gauge boson couplings in $e^+e^- \rightarrow W^+W^-$ using W polarizations with polarized beams*, *Phys. Rev. D* **101** no. 7, (2020) 075044, [arXiv:1909.05496 \[hep-ph\]](#).
- [35] S. S. Biswal, M. Patra, and S. Raychaudhuri, *Anomalous Triple Gauge Vertices at the Large Hadron-Electron Collider*, [arXiv:1405.6056 \[hep-ph\]](#).
- [36] I. T. Cakir, O. Cakir, A. Senol, and A. T. Tasci, *Search for anomalous $WW\gamma$ and WWZ couplings with polarized e -beam at the LHeC*, *Acta Phys. Polon. B* **45** no. 10, (2014) 1947, [arXiv:1406.7696 \[hep-ph\]](#).
- [37] R. Li, X.-M. Shen, K. Wang, T. Xu, L. Zhang, and G. Zhu, *Probing anomalous $WW\gamma$ triple gauge bosons coupling at the LHeC*, *Phys. Rev. D* **97** no. 7, (2018) 075043, [arXiv:1711.05607 \[hep-ph\]](#).
- [38] S. Kumar and P. Poullose, *Probing $WW\gamma$ coupling through $e^-\gamma \rightarrow \nu_e W^-$ at ILC*, *Int. J. Mod. Phys. A* **30** no. 36, (2015) 1550215, [arXiv:1501.01380 \[hep-ph\]](#).
- [39] U. Baur and D. Zeppenfeld, *Unitarity Constraints on the Electroweak Three Vector Boson Vertices*, *Phys. Lett. B* **201** (1988) 383–389.
- [40] L. J. Dixon, Z. Kunszt, and A. Signer, *Vector boson pair production in hadronic collisions at order α_s : Lepton correlations and anomalous couplings*, *Phys. Rev. D* **60** (1999) 114037, [arXiv:hep-ph/9907305 \[hep-ph\]](#).
- [41] A. Falkowski, M. Gonzalez-Alonso, A. Greljo, D. Marzocca, and M. Son, *Anomalous Triple Gauge Couplings in the Effective Field Theory Approach at the LHC*, *JHEP* **02** (2017) 115, [arXiv:1609.06312 \[hep-ph\]](#).
- [42] A. Azatov, J. Elias-Miro, Y. Reyimuaji, and E. Venturini, *Novel measurements of anomalous triple gauge couplings for the LHC*, *JHEP* **10** (2017) 027, [arXiv:1707.08060 \[hep-ph\]](#).
- [43] A. Azatov, D. Barducci, and E. Venturini, *Precision diboson measurements at hadron colliders*, *JHEP* **04** (2019) 075, [arXiv:1901.04821 \[hep-ph\]](#).
- [44] R. Roth, F. Campanario, S. Sapeta, and D. Zeppenfeld, *Anomalous couplings in WZ production beyond NLO QCD*, *PoS LHCP2016* (2016) 141, [arXiv:1612.03577 \[hep-ph\]](#).
- [45] A. Butter, O. J. P. Éboli, J. Gonzalez-Fraile, M. C. Gonzalez-Garcia, T. Plehn, and M. Rauch, *The Gauge-Higgs Legacy of the LHC Run I*, *JHEP* **07** (2016) 152, [arXiv:1604.03105 \[hep-ph\]](#).
- [46] A. Biekötter, T. Corbett, and T. Plehn, *The Gauge-Higgs Legacy of the LHC Run II*, *SciPost Phys.* **6** (2019) 064, [arXiv:1812.07587 \[hep-ph\]](#).

- [47] J. Baglio, S. Dawson, and I. M. Lewis, *An NLO QCD effective field theory analysis of W^+W^- production at the LHC including fermionic operators*, *Phys. Rev.* **D96** no. 7, (2017) 073003, [arXiv:1708.03332 \[hep-ph\]](#).
- [48] H. T. Li and G. Valencia, *CP violating anomalous couplings in W jet production at the LHC*, *Phys. Rev.* **D96** no. 7, (2017) 075014, [arXiv:1708.04402 \[hep-ph\]](#).
- [49] D. Bhatia, U. Maitra, and S. Raychaudhuri, *Pinning down anomalous $WW\gamma$ couplings at the LHC*, *Phys. Rev.* **D99** no. 9, (2019) 095017, [arXiv:1804.05357 \[hep-ph\]](#).
- [50] M. Chiesa, A. Denner, and J.-N. Lang, *Anomalous triple-gauge-boson interactions in vector-boson pair production with RECOLA2*, *Eur. Phys. J.* **C78** no. 6, (2018) 467, [arXiv:1804.01477 \[hep-ph\]](#).
- [51] J. Baglio, S. Dawson, and I. M. Lewis, *NLO effects in EFT fits to W^+W^- production at the LHC*, *Phys. Rev.* **D99** no. 3, (2019) 035029, [arXiv:1812.00214 \[hep-ph\]](#).
- [52] J. Baglio, S. Dawson, and S. Homiller, *QCD corrections in Standard Model EFT fits to WZ and WW production*, *Phys. Rev. D* **100** no. 11, (2019) 113010, [arXiv:1909.11576 \[hep-ph\]](#).
- [53] **OPAL** Collaboration, G. Abbiendi *et al.*, *Measurement of W boson polarizations and CP violating triple gauge couplings from W^+W^- production at LEP*, *Eur. Phys. J.* **C19** (2001) 229–240, [arXiv:hep-ex/0009021 \[hep-ex\]](#).
- [54] **OPAL** Collaboration, G. Abbiendi *et al.*, *Measurement of charged current triple gauge boson couplings using W pairs at LEP*, *Eur. Phys. J.* **C33** (2004) 463–476, [arXiv:hep-ex/0308067 \[hep-ex\]](#).
- [55] **DELPHI** Collaboration, J. Abdallah *et al.*, *Study of W boson polarisations and Triple Gauge boson Couplings in the reaction $e^+e^- \rightarrow W^+W^-$ at LEP 2*, *Eur. Phys. J.* **C54** (2008) 345–364, [arXiv:0801.1235 \[hep-ex\]](#).
- [56] **DELPHI, OPAL, LEP Electroweak, ALEPH, L3** Collaboration, S. Schael *et al.*, *Electroweak Measurements in Electron-Positron Collisions at W -Boson-Pair Energies at LEP*, *Phys. Rept.* **532** (2013) 119–244, [arXiv:1302.3415 \[hep-ex\]](#).
- [57] **CDF** Collaboration, T. Aaltonen *et al.*, *Limits on Anomalous Triple Gauge Couplings in $p\bar{p}$ Collisions at $\sqrt{s} = 1.96$ -TeV*, *Phys. Rev.* **D76** (2007) 111103, [arXiv:0705.2247 \[hep-ex\]](#).
- [58] **D0** Collaboration, V. M. Abazov *et al.*, *Limits on anomalous trilinear gauge boson couplings from WW , WZ and $W\gamma$ production in $p\bar{p}$ collisions at $\sqrt{s} = 1.96$ TeV*, *Phys. Lett.* **B718** (2012) 451–459, [arXiv:1208.5458 \[hep-ex\]](#).
- [59] **ATLAS** Collaboration, M. Aaboud *et al.*, *Measurement of $WW/WZ \rightarrow \ell\nu qq'$ production with the hadronically decaying boson reconstructed as one or two jets in pp collisions at $\sqrt{s} = 8$ TeV with ATLAS, and constraints on anomalous gauge couplings*, *Eur. Phys. J.* **C77** no. 8, (2017) 563, [arXiv:1706.01702 \[hep-ex\]](#).
- [60] **CMS** Collaboration, A. M. Sirunyan *et al.*, *Search for anomalous couplings in boosted $WW/WZ \rightarrow \ell\nu q\bar{q}$ production in proton-proton collisions at $\sqrt{s} = 8$ TeV*, *Phys. Lett.* **B772** (2017) 21–42, [arXiv:1703.06095 \[hep-ex\]](#).
- [61] **ATLAS** Collaboration, M. Aaboud *et al.*, *Measurements of electroweak Wjj production and constraints on anomalous gauge couplings with the ATLAS detector*, *Eur. Phys. J.* **C77** no. 7, (2017) 474, [arXiv:1703.04362 \[hep-ex\]](#).
- [62] **CMS** Collaboration, V. Khachatryan *et al.*, *Measurement of the WZ production cross section in pp*

- collisions at $\sqrt{s} = 7$ and 8 TeV and search for anomalous triple gauge couplings at $\sqrt{s} = 8$ TeV, *Eur. Phys. J. C* **77** no. 4, (2017) 236, [arXiv:1609.05721 \[hep-ex\]](#).
- [63] **ATLAS** Collaboration, G. Aad *et al.*, Measurements of $W^{\pm}Z$ production cross sections in pp collisions at $\sqrt{s} = 8$ TeV with the ATLAS detector and limits on anomalous gauge boson self-couplings, *Phys. Rev. D* **93** no. 9, (2016) 092004, [arXiv:1603.02151 \[hep-ex\]](#).
 - [64] **ATLAS** Collaboration, G. Aad *et al.*, Measurement of total and differential $W^{+}W^{-}$ production cross sections in proton-proton collisions at $\sqrt{s} = 8$ TeV with the ATLAS detector and limits on anomalous triple-gauge-boson couplings, *JHEP* **09** (2016) 029, [arXiv:1603.01702 \[hep-ex\]](#).
 - [65] **CMS** Collaboration, S. Chatrchyan *et al.*, Measurement of the $W^{+}W^{-}$ Cross section in pp Collisions at $\sqrt{s} = 7$ TeV and Limits on Anomalous $WW\gamma$ and WWZ couplings, *Eur. Phys. J. C* **73** no. 10, (2013) 2610, [arXiv:1306.1126 \[hep-ex\]](#).
 - [66] **CMS** Collaboration, P. Rebello Teles, Search for anomalous gauge couplings in semi-leptonic decays of $WW\gamma$ and $WZ\gamma$ in pp collisions at $\sqrt{s} = 8$ TeV, in *Meeting of the APS Division of Particles and Fields (DPF 2013) Santa Cruz, California, USA, August 13-17, 2013*. 2013. [arXiv:1310.0473 \[hep-ex\]](#).
<https://inspirehep.net/record/1256468/files/arXiv:1310.0473.pdf>.
 - [67] **ATLAS** Collaboration, G. Aad *et al.*, Measurement of $W^{+}W^{-}$ production in pp collisions at $\sqrt{s} = 7$ TeV with the ATLAS detector and limits on anomalous WWZ and $WW\gamma$ couplings, *Phys. Rev. D* **87** no. 11, (2013) 112001, [arXiv:1210.2979 \[hep-ex\]](#). [Erratum: *Phys. Rev. D* **88**, no. 7, 079906(2013)].
 - [68] **CMS** Collaboration, S. Chatrchyan *et al.*, Measurement of the sum of WW and WZ production with W +dijet events in pp collisions at $\sqrt{s} = 7$ TeV, *Eur. Phys. J. C* **73** no. 2, (2013) 2283, [arXiv:1210.7544 \[hep-ex\]](#).
 - [69] **ATLAS** Collaboration, G. Aad *et al.*, Measurements of $W\gamma$ and $Z\gamma$ production in pp collisions at $\sqrt{s}=7$ TeV with the ATLAS detector at the LHC, *Phys. Rev. D* **87** no. 11, (2013) 112003, [arXiv:1302.1283 \[hep-ex\]](#). [Erratum: *Phys. Rev. D* **91**, no. 11, 119901(2015)].
 - [70] **CMS** Collaboration, S. Chatrchyan *et al.*, Measurement of the $W\gamma$ and $Z\gamma$ inclusive cross sections in pp collisions at $\sqrt{s} = 7$ TeV and limits on anomalous triple gauge boson couplings, *Phys. Rev. D* **89** no. 9, (2014) 092005, [arXiv:1308.6832 \[hep-ex\]](#).
 - [71] **CMS** Collaboration, A. M. Sirunyan *et al.*, Electroweak production of two jets in association with a Z boson in proton-proton collisions at $\sqrt{s} = 13$ TeV, *Eur. Phys. J. C* **78** no. 7, (2018) 589, [arXiv:1712.09814 \[hep-ex\]](#).
 - [72] **CMS** Collaboration, A. M. Sirunyan *et al.*, Search for anomalous triple gauge couplings in WW and WZ production in lepton + jet events in proton-proton collisions at $\sqrt{s} = 13$ TeV, *JHEP* **12** (2019) 062, [arXiv:1907.08354 \[hep-ex\]](#).
 - [73] **CMS** Collaboration, A. M. Sirunyan *et al.*, Measurement of electroweak production of a W boson in association with two jets in proton-proton collisions at $\sqrt{s} = 13$ TeV, *Eur. Phys. J. C* **80** no. 1, (2020) 43, [arXiv:1903.04040 \[hep-ex\]](#).
 - [74] **CMS** Collaboration, A. M. Sirunyan *et al.*, Measurements of the $pp \rightarrow WZ$ inclusive and differential production cross section and constraints on charged anomalous triple gauge couplings at $\sqrt{s} = 13$ TeV, *JHEP* **04** (2019) 122, [arXiv:1901.03428 \[hep-ex\]](#).
 - [75] T. Corbett, O. J. P. Éboli, J. Gonzalez-Fraile, and M. C. Gonzalez-Garcia, *Determining Triple Gauge*

- Boson Couplings from Higgs Data*, *Phys. Rev. Lett.* **111** (2013) 011801, [arXiv:1304.1151 \[hep-ph\]](#).
- [76] C. Bourrely, J. Soffer, and E. Leader, *Polarization Phenomena in Hadronic Reactions*, *Phys. Rept.* **59** (1980) 95–297.
- [77] I. Ots, H. Uibo, H. Liivat, R. Saar, and R. K. Loide, *Possible anomalous ZZ gamma and Z gamma gamma couplings and Z boson spin orientation in $e^+e^- \rightarrow Z\gamma$* , *Nucl. Phys.* **B702** (2004) 346–356.
- [78] F. Boudjema and R. K. Singh, *A Model independent spin analysis of fundamental particles using azimuthal asymmetries*, *JHEP* **07** (2009) 028, [arXiv:0903.4705 \[hep-ph\]](#).
- [79] J. A. Aguilar-Saavedra and J. Bernabeu, *Breaking down the entire W boson spin observables from its decay*, *Phys. Rev.* **D93** no. 1, (2016) 011301, [arXiv:1508.04592 \[hep-ph\]](#).
- [80] R. Rahaman and R. K. Singh, *On polarization parameters of spin-1 particles and anomalous couplings in $e^+e^- \rightarrow ZZ/Z\gamma$* , *Eur. Phys. J.* **C76** no. 10, (2016) 539, [arXiv:1604.06677 \[hep-ph\]](#).
- [81] J. Nakamura, *Polarisations of the Z and W bosons in the processes $pp \rightarrow ZH$ and $pp \rightarrow W^\pm H$* , *JHEP* **08** (2017) 008, [arXiv:1706.01816 \[hep-ph\]](#).
- [82] F. M. Renard, *Polarization effects due to dark matter interaction between massive standard particles*, [arXiv:1802.10313 \[hep-ph\]](#).
- [83] F. M. Renard, *Z Polarization in $e^+e^- \rightarrow t\bar{t}Z$ for testing the top quark mass structure and the presence of final interactions*, [arXiv:1803.10466 \[hep-ph\]](#).
- [84] F. M. Renard, *W polarization in e^+e^- , gluon-gluon and $\gamma\gamma \rightarrow Wt\bar{b}$ for testing the top quark mass structure and the presence of final interactions*, [arXiv:1807.00621 \[hep-ph\]](#).
- [85] F. M. Renard, *Further tests of special interactions of massive particles from the Z polarization rate in $e^+e^- \rightarrow Zt\bar{t}$ and in $e^+e^- \rightarrow ZW^+W^-$* , [arXiv:1808.05429 \[hep-ph\]](#).
- [86] F. M. Renard, *Z polarization in $e^+e^- \rightarrow ZWW$ for testing special interactions of massive particles*, [arXiv:1807.08938 \[hep-ph\]](#).
- [87] J. A. Aguilar-Saavedra, J. Bernab  , V. A. Mitsou, and A. Segarra, *The Z boson spin observables as messengers of new physics*, *Eur. Phys. J.* **C77** no. 4, (2017) 234, [arXiv:1701.03115 \[hep-ph\]](#).
- [88] S. Behera, R. Islam, M. Kumar, P. Poulou  , and R. Rahaman, *Fingerprinting the Top quark FCNC via anomalous Ztq couplings at the LHeC*, *Phys. Rev.* **D100** no. 1, (2019) 015006, [arXiv:1811.04681 \[hep-ph\]](#).
- [89] R. Rahaman and R. K. Singh, *On the choice of beam polarization in $e^+e^- \rightarrow ZZ/Z\gamma$ and anomalous triple gauge-boson couplings*, *Eur. Phys. J.* **C77** no. 8, (2017) 521, [arXiv:1703.06437 \[hep-ph\]](#).
- [90] R. Rahaman and R. K. Singh, *Anomalous triple gauge boson couplings in ZZ production at the LHC and the role of Z boson polarizations*, *Nuclear Physics B* **948** (2019) 114754, [arXiv:1810.11657 \[hep-ph\]](#).
- [91] W. J. Stirling and E. Vryonidou, *Electroweak gauge boson polarisation at the LHC*, *JHEP* **07** (2012) 124, [arXiv:1204.6427 \[hep-ph\]](#).
- [92] J. Baglio and N. Le Duc, *Fiducial polarization observables in hadronic WZ production: A next-to-leading order QCD+EW study*, *JHEP* **04** (2019) 065, [arXiv:1810.11034 \[hep-ph\]](#).
- [93] J. Baglio and L. D. Ninh, *Polarization observables in WZ production at the 13 TeV LHC: Inclusive case*, *Commun. Phys.* **30** no. 1, (2020) 35–47, [arXiv:1910.13746 \[hep-ph\]](#).

- [94] **ATLAS** Collaboration, M. Aaboud *et al.*, *Measurement of $W^{\pm}Z$ production cross sections and gauge boson polarisation in pp collisions at $\sqrt{s} = 13$ TeV with the ATLAS detector*, *Eur. Phys. J. C* **79** no. 6, (2019) 535, [arXiv:1902.05759 \[hep-ex\]](#).
- [95] M. Grazzini, S. Kallweit, and M. Wiesemann, *Fully differential NNLO computations with MATRIX*, *Eur. Phys. J. C* **78** no. 7, (2018) 537, [arXiv:1711.06631 \[hep-ph\]](#).
- [96] J. Alwall, R. Frederix, S. Frixione, V. Hirschi, F. Maltoni, O. Mattelaer, H. S. Shao, T. Stelzer, P. Torrielli, and M. Zaro, *The automated computation of tree-level and next-to-leading order differential cross sections, and their matching to parton shower simulations*, *JHEP* **07** (2014) 079, [arXiv:1405.0301 \[hep-ph\]](#).
- [97] M. Grazzini, S. Kallweit, D. Rathlev, and M. Wiesemann, *$W^{\pm}Z$ production at the LHC: fiducial cross sections and distributions in NNLO QCD*, *JHEP* **05** (2017) 139, [arXiv:1703.09065 \[hep-ph\]](#).
- [98] **CMS** Collaboration, V. Khachatryan *et al.*, *Measurement of the WZ production cross section in pp collisions at $\sqrt{s} = 13$ TeV*, *Phys. Lett. B* **766** (2017) 268–290, [arXiv:1607.06943 \[hep-ex\]](#).
- [99] M. Grazzini, S. Kallweit, D. Rathlev, and M. Wiesemann, *$W^{\pm}Z$ production at hadron colliders in NNLO QCD*, *Phys. Lett. B* **761** (2016) 179–183, [arXiv:1604.08576 \[hep-ph\]](#).
- [100] F. Cascioli, P. Maierhöfser, and S. Pozzorini, *Scattering Amplitudes with Open Loops*, *Phys. Rev. Lett.* **108** (2012) 111601, [arXiv:1111.5206 \[hep-ph\]](#).
- [101] A. Denner, S. Dittmaier, and L. Hofer, *Collier: a fortran-based Complex One-Loop Library in Extended Regularizations*, *Comput. Phys. Commun.* **212** (2017) 220–238, [arXiv:1604.06792 \[hep-ph\]](#).
- [102] T. Gehrmann, A. von Manteuffel, and L. Tancredi, *The two-loop helicity amplitudes for $q\bar{q}' \rightarrow V_1 V_2 \rightarrow 4$ leptons*, *JHEP* **09** (2015) 128, [arXiv:1503.04812 \[hep-ph\]](#).
- [103] S. Catani, L. Cieri, D. de Florian, G. Ferrera, and M. Grazzini, *Vector boson production at hadron colliders: hard-collinear coefficients at the NNLO*, *Eur. Phys. J. C* **72** (2012) 2195, [arXiv:1209.0158 \[hep-ph\]](#).
- [104] S. Catani and M. Grazzini, *An NNLO subtraction formalism in hadron collisions and its application to Higgs boson production at the LHC*, *Phys. Rev. Lett.* **98** (2007) 222002, [arXiv:hep-ph/0703012 \[hep-ph\]](#).
- [105] **NNPDF** Collaboration, R. D. Ball *et al.*, *Parton distributions for the LHC Run II*, *JHEP* **04** (2015) 040, [arXiv:1410.8849 \[hep-ph\]](#).
- [106] A. Alloul, N. D. Christensen, C. Degrande, C. Duhr, and B. Fuks, *FeynRules 2.0 - A complete toolbox for tree-level phenomenology*, *Comput. Phys. Commun.* **185** (2014) 2250–2300, [arXiv:1310.1921 \[hep-ph\]](#).
- [107] **ATLAS** Collaboration, M. Aaboud *et al.*, *Measurement of the $W^{\pm}Z$ boson pair-production cross section in pp collisions at $\sqrt{s} = 13$ TeV with the ATLAS Detector*, *Phys. Lett. B* **762** (2016) 1–22, [arXiv:1606.04017 \[hep-ex\]](#).
- [108] V. Arunprasath, R. M. Godbole, and R. K. Singh, *Polarization of a top quark produced in the decay of a gluino or a stop in an arbitrary frame*, *Phys. Rev. D* **95** no. 7, (2017) 076012, [arXiv:1612.03803 \[hep-ph\]](#).
- [109] A. Velusamy and R. K. Singh, *Polarization of a vector boson produced in decay of a heavy fermion in an arbitrary frame*, *Phys. Rev. D* **98** no. 5, (2018) 053009, [arXiv:1805.00876 \[hep-ph\]](#).

- [110] A. Lewis, *GetDist: Kernel Density Estimation*, [url: .http://cosmologist.info/notes/GetDist.pdf](http://cosmologist.info/notes/GetDist.pdf),
Homepage <http://getdist.readthedocs.org/en/latest/index.html> .
- [111] S. Buddenbrock, A. S. Cornell, Y. Fang, A. Fadol Mohammed, M. Kumar, B. Mellado, and K. G. Tomiwa, *The emergence of multi-lepton anomalies at the LHC and their compatibility with new physics at the EW scale*, *JHEP* **10** (2019) 157, [arXiv:1901.05300](https://arxiv.org/abs/1901.05300) [[hep-ph](#)].